LM-06K145
January 9, 2007

Thermodynamics of Cr_2O_3, $FeCr_2O_4$, $ZnCr_2O_4$ and $CoCr_2O_4$

SE Ziemniak, LM Anovitz, RA Castelli, and WD Porter

Thermodynamics of Cr_2O_3, $FeCr_2O_4$, $ZnCr_2O_4$ and $CoCr_2O_4$

Stephen E. Ziemniak[1,*]

Lawrence M. Anovitz[2]

Roy A. Castelli[1]

Wallace D. Porter[2]

[1]Lockheed Martin Corp., P. O. Box 1072, Schenectady, New York 12301-1072

[2]Oak Ridge National Laboratory, P. O. Box 2008, Oak Ridge, Tennessee 37831-6110

*Corresponding author; e-mail: ziemnia@kapl.gov

(for submittal to J. Chem. Thermo.)

ABSTRACT

High temperature heat capacity measurements were obtained for Cr_2O_3, $FeCr_2O_4$, $ZnCr_2O_4$ and $CoCr_2O_4$ using a differential scanning calorimeter. These data were combined with previously-available, overlapping heat capacity data at temperatures up to 400 K and fitted to 5-parameter Maier-Kelley $C_p(T)$ equations. Expressions for molar entropy were then derived by suitable integration of the Maier-Kelley equations in combination with recent S°(298) evaluations. Finally, a database of high temperature equilibrium measurements on the formation of these oxides was constructed and critically evaluated. Gibbs energies of Cr_2O_3, $FeCr_2O_4$ and $CoCr_2O_4$ were referenced by averaging the most reliable results at reference temperatures of 1100, 1400 and 1373 K, respectively, while Gibbs energies for $ZnCr_2O_4$ were referenced to the results of Jacob [Thermochim. Acta 15 (1976) 79-87] at 1100 K. Thermodynamic extrapolations from the high temperature reference points to 298.15 K by application of the heat capacity correlations gave $\Delta_f G°(298)$ = -1049.96, -1339.40, -1428.35 and -1326.75 kJ mol^{-1} for Cr_2O_3, $FeCr_2O_4$, $ZnCr_2O_4$ and $CoCr_2O_4$, respectively.

Keywords: magnetic materials, oxides, differential scanning calorimetry (DSC), specific heat, thermodynamic properties

Thermodynamics of Cr_2O_3, $FeCr_2O_4$, $ZnCr_2O_4$ and $CoCr_2O_4$

1. INTRODUCTION

The family of transition metal chromites, MCr_2O_4, where M = Fe, Ni and Co and Zn represent ideal constituents of the metal oxide 'skins' that form on iron and nickel base FeNiCr alloys exposed to hydrothermal environments typical of light water nuclear reactors. Presently available compilations of Gibbs energies ($\Delta_f G°$) for Cr_2O_3 and the family of MCr_2O_4 oxides are based on extrapolations of both high-temperature data ($\Delta G°$, $\Delta H°$) and low-temperature data (S°) to room temperature. Unfortunately, most of these extrapolations have been conducted in the absence of experimentally-determined heat capacities, using estimates of uncertain validity.

Tabulated Gibbs energies, for example, for Cr_2O_3, $FeCr_2O_4$, and $CoCr_2O_4$ in Barin [1] rely on estimated, super-ambient heat capacities for these oxide phases; no entry is provided for $ZnCr_2O_4$. Furthermore, the chromium(III) ion-based spinel oxides undergo magnetic transitions at very low temperatures, and additional phenomena associated with the presence of transition metal ions (i.e., Schottky effect) may also contribute to heat capacity anomalies in this low temperature region. Therefore, any low temperature extrapolation of C_p to absolute zero based on application of the Debye equation (C_p % T^3) will be inappropriate and lead to significant underestimation of standard molar entropy, S°(298).

Recent results, obtained within the past decade, have considerably improved the state of knowledge regarding the thermodynamic properties of Cr_2O_3: emf studies ($\Delta_f G°$, $\Delta_f H°$; Holzheid and O'Neill [2]) and low temperature C_p studies (down to 1.5 K; Klemme et al. [3]). New C_p measurements for $FeCr_2O_4$, which extended the temperature range down to 2.5 K [3], confirmed the presence of a magnetic anomaly (at 36.5 K) that had been predicted earlier based on neutron diffraction measurements [4]. Similarly, C_p measurements for $NiCr_2O_4$ [5], $ZnCr_2O_4$ [6] and $CoCr_2O_4$ [7] are now available in the temperature range 0.5 to 400 K. This work has also revealed thermal anomalies, indicative of magnetic transitions in $NiCr_2O_4$ (at 29 K), $ZnCr_2O_4$ (at 12.3 K) and $CoCr_2O_4$ (at 24 K).

Due to these encouraging results, improved estimates for standard molar entropies are now available for Cr_2O_3, $FeCr_2O_4$, $ZnCr_2O_4$ and $CoCr_2O_4$. The present work was undertaken to eliminate the remaining source of uncertainty in extrapolating available super-ambient temperature reaction equilibria to 298.15 K by performing high temperature heat capacity measurements for the above four oxides. Then, by combining the new results with a critical evaluation of the existing database of high temperature reaction equilibria for formation of these oxides, recommended thermodynamic properties are determined for Cr_2O_3, $FeCr_2O_4$, $ZnCr_2O_4$ and $CoCr_2O_4$ at 298.15 K (S°, C_p°, $\Delta_f H°$ and $\Delta_f G°$).

2. HIGH TEMPERATURE HEAT CAPACITY MEASUREMENTS

2.1 Experimental Methodology

The metal oxides examined were synthesized ceramically from high purity single metal oxide powders. Portions of these materials have also been used in solubility studies; see Wesolowski et al. [8] and references cited therein. Descriptions of oxide preparation and characterization are included in individual publications reporting their solubility behavior (cf. Ziemniak et al. [9]). For completeness, a summary of their crystallographic features is given in Table I.

The super-ambient heat capacities of Cr_2O_3, $FeCr_2O_4$, $ZnCr_2O_4$ and $CoCr_2O_4$ were measured using a Netsch differential scanning calorimeter (DSC). In order to prevent oxidation of the materials during the measurement, a reducing atmosphere was maintained in the calorimeter by first evacuating it, backfilling three times with Ar gas, and then performing the measurement under a slowing flowing Ar stream. The argon used was first deoxygenated using a high-temperature Zn oxygen getter to further reduce any potential for sample oxidation.

The same measurement procedure was used for all materials. Each sample was first ground by hand to a powder in an agate mortar. During test runs these powders were pressed into the Pt sample pan by hand. Initially, each sample was dried by heating to 300°C in an Ar stream in a thermal gravimeter for a few minutes. However, examination of several samples processed in this manner showed that no weight changes occurred during this time. As this implied that the amount of water adsorbed onto the powder was too small to affect the C_p results this procedure was discontinued.

Data were first obtained for each phase up to 1050°C using both heating and cooling cycles at a rate of 10°C/min with 30 minute isothermal holds at 400, 700 and 1050°C. An empty Pt pan was used on the reference side, and this pan was not moved between cycles. Each measurement required five heating/cooling cycles. In the first, the empty sample pan was run to serve as a standard. In the second, third and fifth, a sapphire disc was run to serve as a standard. The repetition of this measurement was performed in order to obtain an estimate of the repeatability of the measurement. Initially, this was done without running the sample multiple times, which it was thought, might adversely affect its composition or structure. Later tests, however, showed that these materials were stable under the measurement conditions and sample repetitions were also performed.

Once the first set of runs was completed, a second set was initiated to obtain C_p data at higher temperatures. These were expected to be more difficult, as the DSC is less stable above 1000°C, and thus were run separately. Again, both heating and cooling cycles were used, with the sample heated at 10°C/min., and isothermal holds imposed at 1050, 1400 and 1600°C. As the temperature range from room temperature to 1050°C had to again be traversed for these measurements, additional repetitions of the measurements below 1050°C were performed to further refine the experimental statistics. Data above 1050°C were not obtained for $ZnCr_2O_4$, as the temperatures of the available experiments constraining its Gibbs energy do not exceed 1000°C.

2.2 Data Preprocessing

The aforementioned experiments provided a number of repetitive measurements of C_p for each material. To process these data, the results of each run were first calculated using each of three measurements with the sapphire standard. The results of the heating and cooling cycles for each run were then averaged, and the results compared. An example of this comparison is shown in Figure 1, which shows the raw data for Cr_2O_3. In all cases, results from sapphire 3, which was run after the sample itself, were somewhat different from the remainder. This was probably caused by deformation of the sample pan during sample removal, and the sapphire 3 calculations were therefore not used for further calculations. The remaining results were again averaged, and the standard deviations of this average calculated as a function of temperature. The resultant curves were then compared to the low-temperature C_p data in the literature. Finally, the data were extrapolated by hand to 2000°C (2000 K for the chromites). This was done to place a high-temperature constraint on the fitted C_p curve, which tended to deviate from a reasonable extrapolation unless such a constraint was employed.

Prior to fitting it was necessary to "clean up" the data set by removing certain data points. This was done for several reasons. First, because heating is slower than normal immediately after an isothermal hold, and because the sensitivity of the DSC is directly proportional to heating rate, data points taken immediately after an isothermal hold tended to deviate significantly from the true curve. As the heating and cooling curves each contained these holds, 10-15 data points were deleted on each side of the isothermal hold temperature. Second, examination of the results showed that the higher temperature

data were often unreliable, deviating significantly from the trend of the lower temperature results. These were thus deleted as needed (see discussion below).

The final step in processing the data was to fit it to an equation that can be used to obtain and integrate C_p as a function of temperature. While there are a number of theoretically reasonable choices for this equation, an empirical equation, the extended Maier-Kelley formulation used by Robie and Hemingway [10], was chosen:

$$C_p = A + BT + CT^2 + DT^{-0.5} + ET^{-2} \quad (1)$$

3. RESULTS

A summary of results in terms of fitted Maier-Kelley parameters is provided in Table 2. Calculation of molar entropy (at temperatures above 298.15 K) follows from thermodynamic relationships by integration of C_p/T:

$$S^\circ(T) = S^\circ(298) + \int_{298}^{T} \frac{C_P}{T}\, dT \quad (2)$$

where S°(298) is the standard molar entropy. Values for the latter parameter, determined by suitable integration of low temperature heat capacity measurements in the literature [3, 6, 7], are summarized in Table 3. Upon integrating Eq. (2) with the Maier-Kelley parameters of Eq. (1), it is found that

$$S^\circ(T) = S^\circ(298) + A \ln T + BT + (C/2)T^2 - 2DT^{-0.5} - (E/2)T^{-2} - F \quad (3)$$

where F is the integral of C_p/T evaluated at 298.15 K. A summary of F values is also given in Table 3. Analytical considerations for each material are given below.

3.1 High Temperature C_p and Entropy of Cr_2O_3

Figure 1 shows the unedited data for Cr_2O_3. As noted above, spikes in these data near 400, 700, 1050, and 1400°C are the result of the isothermal holds in the heating and cooling cycles. The separation of the sapphire 3 runs (the three highest C_p runs at low T) and the greater variability in the data above 1050°C is also apparent. Included along the bottom of Fig. 1 is the root-mean-square (rms) deviation of $C_P(T)$ after editing at the isothermal holds. As can be seen, the editing process significantly reduces the scatter in the data. The standard deviation is relatively consistent, and reasonably small up to approximately 1250°C (i.e., < 1%), but increases significantly at higher temperatures (~2% above 1400°C). These results are within the stated accuracy of the DSC ("3% at temperatures below 1400°C, and "5% from 1400 to 1600°C). However, due to the degraded data quality at temperatures above 1400°C, these data were excluded from an initial analysis of the measurements.

Figure 2 summarizes the high-temperature data. The three irregular lines show the average of the edited values for C_p as a function of temperature, and the same data plus or minus two standard deviations. A significant feature of these data is the apparent increase in C_p at temperatures above approximately 1200°C relative to the values predicted by a smooth extrapolation of the lower temperature data. This behavior is reflected in the first smooth fit to the data, the sigmoid curve shown in Fig. 2. The question is whether this trend is real. In metals, such a trend is often observed at higher temperatures due to formation of increased numbers of vacancies (see, for example, the data for Cr metal). Such an effect is not, however, common in oxides. For instance, the

sapphire data used as a standard for these calculations (NIST standard reference material 720) show no such trend. Therefore, to eliminate this probable bias, the data above 1100°C were excluded from the fit of the high-temperature $C_p(T)$ data and the Maier-Kelley parameters for Cr_2O_3 were constrained to give $C_p(2000°C) = 127.67$ J mol^{-1} K^{-1}. The improved, high-temperature, heat capacity extrapolations obtained in this manner are shown as a dot-dashed curve in Fig. 2.

On the other hand, extrapolation of the C_p database to 298.15 K was complicated by the existence of a N**J**el point (ferromagnetic-paramagnetic transition) in Cr_2O_3 at 306.98 K. Although the transition occurs near room temperature, it is rather diffuse and affects heat capacity over a rather broad temperature interval, which makes application of Maier-Kelley parameters nearly inappropriate. A pragmatic approach was taken for separating the baseline contribution from the λ-anomaly by combining our processed measurements, recorded above 400 K, with previous results in the transition [11] and low temperature [3] regions, i.e.:

$$C_p = C_p^{\text{baseline}} + C_p^{\text{mag},\lambda} \tag{4}$$

A seamless transition between the latter two databases was created in their region of overlap by excluding the data of Klemme et al. [3] above 303 K (due to a suspected vacuum grease effect); the four divergent data points of Bruce and Cannell [11] below 296 K were also dropped. Deconvolution of the baseline and magnetic contributions was accomplished by simultaneously fitting the Maier-Kelley correlation, Eq. (1), and the Inden model [12] to fit $C_p^{\text{mag},\lambda}$ via

$$C_P^{mag} = 2K^{-}R\left[\tau^m + \frac{1}{3}\tau^{3m} + \frac{1}{5}\tau^{5m}\right] \qquad (\text{for } \tau < 1) \tag{5}$$

$$C_P^{mag} = 2K^+ R\left[\tau^{-n} + \frac{1}{3}\tau^{-3n} + \frac{1}{5}\tau^{-5n}\right]. \qquad (\text{for } \tau > 1) \qquad (6)$$

The Inden model allows for different temperature dependencies below and above the transition point (T_c, $\tau = T/T_c$) and has been applied successfully to other (anti)ferromagnetic oxides such as Fe_2O_3, Fe_3O_4, FeO, NiO and MnO [12 - 14]. Evaluation of four model parameters is required: m, K^-, n and K^+. A summary of the fitted parameters for Cr_2O_3 is given in the footnote in Table 2.

Figure 3 shows that the fitted C_p curve for Cr_2O_3 successfully reproduces both low and high temperature portions of the database ($\sigma = \pm 0.4\%$; only data in the temperature range 250 to 1373 K were considered). Because of the 'smoothing' constraint on C_p applied at 2000°C, it is expected that the fitted Maier-Kelley parameters for Cr_2O_3 summarized in Table 2 will also provide reasonable estimates for $C_p^{baseline}$ at temperatures needed for extrapolation of existing ΔG measurements, i.e., ~1500-1900 K.

The impact of the λ-transition on calculation of molar entropy via Eqs. (2, 3) is to add the integral

$$\int_{298}^{T} \frac{C_P^{mag}}{T} dT = S^{mag}(T) - S^{mag}(298) \qquad (7)$$

Based on previously-derived relationships for the Inden model [12], it is known that (for $\tau > 1$)

$$S^{mag}(T) - S^{mag}(\infty) = -2K^+ R\left[\frac{\tau^{-n}}{n} + \frac{\tau^{-3n}}{9n} + \frac{\tau^{-5n}}{25n}\right] \qquad (8)$$

Provided that T is sufficiently high, this contribution is negligible. On the other hand, the formula for the lower limit (i. e., where $\tau = 298.15/306.99$) is given by

$$S^{mag}(298) - S^{mag}(\infty) = -2K^{-}R\left[C' - \frac{\tau^{m}}{m} - \frac{\tau^{3m}}{9m} - \frac{\tau^{5m}}{25m}\right] - 2K^{+}RD' \qquad (9)$$

where $C' = \frac{1}{m}\left(1 + \frac{1}{9} + \frac{1}{25}\right) = 0.3222$ and $D' = \frac{1}{n}\left(1 + \frac{1}{9} + \frac{1}{25}\right) = 0.1764.$

Upon substituting the indicated values, the added entropy, Eq. (7), becomes 0.1811R.

3.2 High Temperature C_p and Entropy of $FeCr_2O_4$

The results and analysis of our DSC measurements of $FeCr_2O_4$ are shown in Figs. 4-6. Figure 4 shows the edited data, together with their rms deviations, for all temperatures up to 1600°C. Figure 5 shows the average value plus or minus two standard deviations. As can be seen, the results from each of the runs are relatively consistent and the curve has the predictable shape up to approximately 1200°C, after which the rms deviation begins to increase. As done previously to discount the apparent upturn in the (lower quality) C_P data above 1200°C, and to ensure a smooth, bounded extrapolation at higher temperatures, the Maier-Kelley parameters for this material were constrained to give $C_P(2000\ K) = 182.0\ J\ mol^{-1}\ K^{-1}$.

Also included in Fig. 5 are the previous high-temperature heat capacity measurements of Naylor [15]. It is noteworthy that these results are about 5-8% higher than the present DSC results; the difference being beyond the reported measurement uncertainties. The source of this deviation is believed to be due to sample purity/non-stoichiometry effects:

our material was a single phase, cubic oxide that had been synthesized at 1625ºC in a flowing CO_2/CO atmosphere (50/50 vol%) and had a lattice parameter of 8.3780(5) Å. The chromite studied previously [15] had been synthesized in a vacuum at 1300ºC, contained 0.75% silica and had a lattice parameter of 8.358 Å. Since the latter value differs considerably from the presently-accepted value for ferrous chromite in the ICDD database, i.e., 8.379(2) Å per PDF no. 034-0140 [16], we conclude that the material tested by Naylor [15] was not stoichiometrically-pure $FeCr_2O_4$.

Additional judgment was also applied when extrapolating the high-temperature database down to 298.15 K, since the $FeCr_2O_4$ heat capacities obtained using adiabatic calorimetry at near-ambient temperatures (298.15 ±50 K) [3, 17] are higher than those obtained by downward extrapolation of the DSC results. As shown in Fig. 6, data in the region of temperature overlap exhibit a marked separation. Most of the deviation is caused by a marked upturn in C_P reported by Klemme et al. [3] at the upper end of their measured temperature range, as well as a steep decline in C_P at the lower end of our measured temperature range. An analysis of the second derivative of the C_P values reported by Klemme et al. [3] with respect to temperature reveals that the uncharacteristic upturn begins around 310 K. Klemme et al. [3] acknowledge that their C_p measurements in this temperature region were 'compromised by the strongly increasing viscosity of the Apiezon N high vacuum grease' used to mount samples in their calorimeter and excluded data >310 K when developing a C_P vs. T correlation. Such anomalous behavior complicates fitting the high and low-temperature data sets, and makes the measured

S°(298) value somewhat uncertain, since the temperature at which this effect began cannot be determined unambiguously.

Fitting was completed by first removing all of the data Klemme et al. [3] obtained at temperatures above 300 K from the data set to be fitted. Despite this truncation, however, the projection of the remaining low-temperature data to higher temperatures yields values that are still slightly higher than the average of the lowest temperature DSC results (at 340 K). To account for this difference/bias and still yield a smooth fit to the data, the fit was allowed to increase above the average of the measured DSC values, but was constrained at 340 K to remain within two standard deviations of the average. As stated above, a hand-fitted point was also added at 2000 K to constrain the behavior of the fitted curve at high temperatures. This yielded the curve shown in Fig. 6, which was generated from the Maier-Kelley equation using the parameters shown in Table 2.

The above fit reproduces both datasets over the temperature range 200 to 1500 K to within ±0.4% except around 1400 K (where quality of the DSC data had degraded) and the interval around 300 K (where the low and high temperature datasets deviate by as much as 10%). In the latter case, the degree of disagreement is beyond the combined measurement uncertainties, which could indicate that the vacuum grease effect compromised a greater portion of the Ref. [3] data than expected.

Finally, the integration constant for the Maier-Kelley based entropy equation was determined by constraining S°(298) to 152.2 J mol^{-1} K^{-1}. As noted by Klemme et al. [3]

this value (which includes the thermal anomaly at 36.5 K) is more than 6 J mol^{-1} K^{-1} greater than the value used in thermodynamic compilations for $FeCr_2O_4$ prior to 2000.

3.3 High-Temperature C_p and Entropy of $ZnCr_2O_4$

The results and analysis of our DSC measurements of $ZnCr_2O_4$ are shown in Figs. 7 and 8. Because measurements for $ZnCr_2O_4$ were made only up to 1050°C, there are many fewer data for it than for the other three oxides, as only a single heating/cooling cycle was obtained. Figure 8 shows the average DSC results (30 - 1050°C), together with the higher temperature results from the low-temperature adiabatic calorimetric measurements (250 - 400 K) reported in Ref. [6]. As can be seen, the agreement between the two data sets is quite good. Figure 8 also includes the results of a Maier-Kelley fit to these data ($\sigma = \pm 0.4\%$), which includes a hand-fitted constraint at 2000 K.

The fitted Maier-Kelley parameters and required S°(298) value for $ZnCr_2O_4$ are summarized in Tables 2 and 3.

3.4 High-Temperature C_p and Entropy of $CoCr_2O_4$

The results and analysis of our DSC measurements of $CoCr_2O_4$ are shown in Figs. 9 and 10. Figure 9 presents the edited data and their root-mean-square deviations for all temperatures from 50 to 1400°C. Data from 1400 to 1600°C are omitted as they showed extreme instability and had to be discarded during the editing process. Results below 1400°C have, however, a relatively small standard deviation, with no obvious increase above 1050°C as observed in the other data sets. Nonetheless, examination of the

average values in Fig. 10 shows that, above 1050°C the average value appears to drop slightly below the trend at lower temperatures. This behavior is probably due to measurement uncertainty.

Figure 10 compares the DSC results with the higher temperature results from the low-temperature adiabatic calorimetric database [7]. As can be seen, the low-temperature heat capacity measurements yielded C_p values slightly above the average of the DSC data at temperatures up to 400 K (but well within the two sigma uncertainty in the DSC results), but fitting a curve to the average DSC data (50 - 1400°C, with an anchor at 2000 K) would be expected to yield a poor prediction of the higher temperature adiabatic calorimetric results. Therefore, an adjusted fit was obtained which fits the (more accurate) adiabatic calorimetric results from 250 to 400 K and blends smoothly into the DSC results by 450 K. As the adjusted fit is a much better representation of the combined database from 250 to 1673 K ($\sigma = \pm 0.3\%$), this curve has been adopted here (see Table 2).

Table 3 provides the integration constant and standard molar entropy of $CoCr_2O_4$ which allow calculation of S°(T) via Eq. (3).

4. DETERMINATION OF GIBBS ENERGIES

Accurate calculation of the thermodynamics of a given phase at 1 bar (the reference pressure) requires the availability of data on the Gibbs energy or enthalpy of formation from the elements and knowledge of entropy as a function of temperature. Having

determined the high temperature heat capacity and entropy functions for all four phases of interest, it remains to calculate their Gibbs energy and enthalpy from data in the literature. For example, the change in enthalpy for each oxide formation reaction from the elements, $\Delta_f H°$, is determined by integrating the change in heat capacities for the formation reaction:

$$\begin{aligned}\Delta_f H^\circ(T) &= \Delta_f H^\circ(298) + \int_{298}^{T} \Delta_f C_p dT \\ &= \Delta_f H^\circ(298) + a\,T + (b/2)T^2 + (c/3)T^3 \\ &\quad + 2dT^{0.5} - eT^{-1} - g\end{aligned} \tag{10}$$

where the lower case letter designators represent changes in the upper case Maier-Kelley letter designators given in Tables 2 and 6, and g is the value of the heat capacity integral at 298.15 K. Gibbs energies follow from the definition

$$\begin{aligned}\Delta_f G^\circ(T) &= \Delta_f H^\circ(T) - T\Delta_f S^\circ(T) \\ &= \Delta_f G^\circ(298) - (T - 298.15)\,\Delta_f S^\circ(298) - g \\ &\quad - aT(\ln T - 1) - (b/2)\,T^2 - (c/6)\,T^3 \\ &\quad + (4d)\,T^{0.5} - (e/2)T^{-1} + f\,T\end{aligned} \tag{11}$$

Slight modifications of Eqs. (10, 11) are required for the Cr_2O_3 analysis, however, since the effect of its magnetic transition needs to be accounted for. For example, an additional term is required in the enthalpy equation, Eq. (10), as

$$\int_{298}^{T} C_P^{mag} dT = H^{mag}(T) - H^{mag}(298) \tag{12}$$

As demonstrated in the entropy calculation, provided that T is sufficiently high, the upper limit may be neglected and the lower limit evaluated from the Inden model (see [12]):

$$H^{mag}(298) = -2K^- RT_c \left[A' - \frac{\tau^{1+m}}{1+m} - \frac{\tau^{1+3m}}{3(1+3m)} - \frac{\tau^{1+5m}}{5(1+5m)} \right] + 2K^+ RT_c B' \tag{13}$$

where $A' = \frac{1}{1+m} + \frac{1}{3(1+3m)} + \frac{1}{5(1+5m)} = 0.2577$ and $B' = \frac{1}{1-n} + \frac{1}{3(1-3n)} + \frac{1}{5(1-5n)} = -0.2052$

Substituting the fitted Inden model parameters for Cr_2O_3 provided in Table 2 into the above allows Eq. (12) to be evaluated as 659.96 J mol^{-1}.

The actual extrapolation process during which $\Delta_f G°(298)$ is determined requires an evaluation of competing, often discrepant results, in order to select the most accurate high temperature reference value. The selection process for each of the four oxides is discussed below; the extrapolated $\Delta_f G°(298)$ values are summarized in Table 10.

4.1 Gibbs Energies of Cr_2O_3

The thermodynamic properties of Cr_2O_3 have been under investigation for nearly a century, beginning with the work of Russell [18], who measured the heat capacity of Cr_2O_3 from 137 to 299 K. Table 4 lists the various sets of experimental data obtained to date: (1) Gibbs energies, (2) $\Delta_f H°(298)$ measurements and (3) C_P measurements. Two types of high temperature experiments have been employed to determine Gibbs energies: gas mixing/equilibration studies and emf measurements using solid electrolytes. Perhaps not surprisingly, serious disagreements have arisen among the various sources of data. Fortunately, most of these differences have been chronologically resolved by subsequent improvements in experimental equipment/methodology which have resulted in improved data quality.

As shown in Table 4, most of the gas equilibrium and emf studies had been completed by the late 1970s, and a consensus had been established by Chase [40] who identified obvious outliers and their suspected causes: non-equilibrium and ionic conduction effects. As noted in Table 4, the solid electrolyte results of Tretjakow and Schmalzreid [25] and Pugliese and Fitterer [26] should be ignored because the fO_2 of reaction (15) is well below the range of oxygen fugacities over which the electrolytes employed act as purely ionic conductors. At 1000°C, the electronic conduction domain for Y_2O_3-ThO_2 electrolytes is between oxygen fugacities of 10^{-6} and 10^{-25}, and that of CaO-ZrO_2 electrolytes is between 10^{5} and 10^{-18}. The upper limit is set by the onset (> 1%) at high oxygen fugacities of p-type semiconduction caused by diffusion of defects which are predominantly interstitial anions and electron holes. The lower limit is set by the onset of n-type semiconduction due to diffusion of defects which are predominantly oxygen vacancies and electrons. In the intermediate electronic conduction region, however, the predominant defects are oxygen vacancies and oxygen interstitials, and thus in this region the current is due almost solely to oxygen diffusion and the voltage measured reflects only the oxygen potential difference across the cell. The limits of this region are, however, also affected by temperature. For Y_2O_3-ThO_2 electrolytes the upper limit is essentially constant with temperature, but the oxygen fugacity of the lower limit increases rapidly with increasing temperature and the electronic conduction region pinches out at approximately 1600 - 1700°C. Both the upper and lower limits of the electronic conduction region of CaO-ZrO_2 electrolytes become more constraining with increasing temperature, and its limit extends up to approximately 2100°C at an fO_2 near 10^{-4} [41].

Among the emf studies using Y_2O_3-ThO_2 electrolytes only the upper temperature studies of Holzheid and O'Neill [2] appear to exceed these limits.

Among the electrolyte studies performed using an yttria-doped thoria electrolyte there is better agreement but, as pointed out by Anovitz [42], the larger the oxygen fugacity difference between the reference and unknown sides of such cells, the larger the error due to electrode polarization (see also discussion in Worrell [41]). Thus, the data of Holzheid and O'Neill [2] are likely to be closer to the actual values than those of Mazandarany and Pehlke [28] or Jacob [29], as the oxygen fugacity of the Fe-FeO reference used is significantly closer to that of reaction (14) than the Co-CoO buffer, although it is still approximately 5 log units more oxidizing.

Figure 11 shows $\Delta_f G°(T)$ values for the formation reaction of Cr_2O_3 from the elements

$$2Cr + 3/2O_2 = Cr_2O_3 \qquad (14)$$

The results shown are derived from both high temperature emf and gas mixing data over the temperature ranges of the experiments. They are believed to be the most reliable and have been independently replicated. As can be seen, there is approximately a 7 kJ mol^{-1} spread in Gibbs energies within the actual temperature range of the measurements. Among the emf data, those of Mazandarany and Pehlke [28] and Jacob [29] have not been corrected to the recent Co-CoO values of O'Neill and Pownceby [43], as was done by Holzheid and O'Neill [2], however, as it was felt to be more consistent to reference each experiment to results obtained in their own laboratories.

Mindful of the limitations in the measurement of high temperature equilibria discussed above, and considering the temperature ranges represented by the various studies, a decision was made (somewhat arbitrarily) to fix $\Delta_f G°(T)$ to a reference value at 1100 K determined by averaging the results of Jeannin et al. [22] (-839.96 ±1.26 kJ mol^{-1}), Mazandarany and Pehlke [28] (-840.32 ±1.46 kJ mol^{-1}), Jacob [29] (-840.55 ±0.90 kJ mol^{-1}), Zabeivorota et al. [30] (-843.26 ±3.14 kJ mol^{-1}) and Holzheid and O'Neill [2] (-838.78 ±0.26 kJ mol^{-1}). In this manner, it is found that $\Delta_f G°(1100\ K) = -840.58 \pm 1.48$ kJ mol^{-1} for reaction (14). Application of the heat capacity correlations for Cr_2O_3 (Table 2), Cr (Tables 6, 7) and O_2 (Table 6) allows the thermodynamic extrapolation to 298.15 K to be completed via Eq. (11):

$$\Delta_f G°(1100\ K) = \Delta_f G°(298) - 801.85\,\Delta_f S°(298) - 9131.37 \text{ J mol}^{-1}$$

It is noteworthy that λ-transitions in Cr_2O_3 and Cr contribute -996.38 and 2(19.81) J mol^{-1}, respectively, to the above extrapolation. The calculation is completed by substituting the standard molar entropy change for reaction (14) given in Table 5: $\Delta_f G°(298) = -1049.96$ kJ mol^{-1}.

Included in Fig. 11 are the thermodynamically-extrapolated Gibbs energies of reaction (14), calculated by applying Eqs. (10, 11) using the values determined for $\Delta_f G°(298)$ and $\Delta_f S°(298)$, and accounting for the λ-transitions using Eqs. (7, 12). This comparison illustrates the very close agreement between thermodynamic extrapolation and the consensus, high-quality, literature results. When the deviations are plotted on an expanded scale (see Fig. 12), the deviations are seen to be non-uniformly distributed and

exhibit a slight temperature dependence. While some adjustments are possible within the uncertainties in the measurements, these are limited, and will affect other reactions calculated below. As will be seen, such adjustments are not possible without offsetting adjustments in parameters associated with the formation of the other chromites, especially $ZnCr_2O_4$. We have therefore chosen not to adjust the measured parameters for Cr_2O_3, but to retain a reference point for the Gibbs energy that generally bisects the various experimental determinations. This approach most clearly depicts the true remaining uncertainties in the Gibbs energy of Cr_2O_3 and yields the $\Delta_f G°(298)$ value given in Table 10.

4.2 Gibbs Energies of $FeCr_2O_4$

At least 13 studies are available which constrain the Gibbs energy of $FeCr_2O_4$. These are summarized in Table 8, and shown relative to the data of Jacob and Alcock [55] in Fig. 13. The studies can be generally divided into those performed using the emf technique and those performed in some other manner. As can be seen in Fig. 13, there are significant discrepancies among the various studies. Some are relatively easily explained, others are not. For the gas mixing experiments, the key to understanding the differences lies in the concept of experimental reversals. Only reaction equilibria bracketed by positive reaction from both directions, using the phases involved in the reaction as starting materials, can be said to have been experimentally located. Experiments which drive the reaction in only one direction are incompletely constrained, and those which begin with other materials (such as gels) cannot be used to imply the location of the equilibrium at all.

The experiments of Kunnmann et al. [49] attempted to find the CO/CO_2 ratio at which chromite formed from iron and Cr_2O_3. This should have provided a half reversal, constraining the maximum oxygen fugacity at which the reaction:

$$Fe + 1/2O_2 + Cr_2O_3 = FeCr_2O_4 \quad (15)$$

occurs at a given temperature. In fact, the values obtained are much higher than those of the other authors ($\Delta_f G°$ differences range from 22.9 kJ mol^{-1} to 24.5 kJ mol^{-1} more positive than the values provided by the fitted equation of Jacob and Alcock [55]), requiring an increase in the CO/CO_2 ratio of approximately three orders of magnitude. This suggests that either: (1) the gas flow system used was incapable of accurately measuring the large ratios involved, (2) one or the other of the gases used was not pure, containing either the other carbon species or, more likely, sufficient oxygen to significantly affect fO_2 at the relatively reducing conditions of this reaction, or (3) significant overstepping was necessary for the reaction to occur.

The gas experiments performed by Novokhatskii and Lenev [23] are the only ones available which suggest that reaction (15) lies at an oxygen fugacity more reducing than suggested by the emf experiments of Jacob and Alcock [55]. These were performed by flowing dried hydrogen over hot $FeCr_2O_4$ (or Cr_2O_3) and measuring the water content of the resulting gas. In this classic half reversal method, water is formed, but there is no assurance that the amount of water produced has reached the equilibrium value. Barring complications, the water content of the gas should not be greater than the equilibrium value, but it may be less. Novokhatskii and Lenev [23] did not perform the other half

reversal, forming hydrogen from reaction of water with chromite. Thus, their experiments can only be taken as limiting the location of the reaction on one side, and the fO_2 of reaction (15) should lie at or above the values measured - exactly the results obtained.

By contrast, Katsura and Muan [50] appear to have reversed reaction (15). This was achieved by placing the solids in a controlled atmosphere, slowly varying the oxygen fugacity, and: (1) observing the oxygen fugacity at which a mixture of $FeCr_2O_4$ and Cr_2O_3 began to lose weight and, (2) finding the oxygen fugacity at which a mixture of metallic iron and Cr_2O_3 began to gain weight. This value should be correct, within the uncertainties in their measurements, and assuming that their materials were stoichiometric and appropriately ordered. In fact, the data point obtained by Katsura and Muan [50] falls almost exactly on the extrapolation of the emf data of Rezukhina et al. [52].

Chen and Chipman [48] reacted Fe-Cr metal melts with H_2O/H_2 vapor of a fixed composition in Cr_2O_3 and $FeCr_2O_4$ crucibles, and measured the final Cr content of the melt. Because of experimental difficulties all reactions began on the low-Cr side of the reaction equilibrium. The Gibbs energy of formation from the oxides of $FeCr_2O_4$ was determined from the H_2O/H_2 and Fe/Cr ratios of the intersection of the Cr_2O_3 and $FeCr_2O_4$ reactions. This determination is, therefore, not only a half reversal, only limiting the maximum stability of $FeCr_2O_4$, but suffers from uncertainties due to the low angle of intersection of the two reactions and uncertainties in the mixing properties of the molten metal.

Hino et al. [51] equilibrated liquid silver in a crucible constructed from Cr_2O_3 and $FeCr_2O_4$, where the oxygen potential was controlled by a CO-CO_2 gas mixture:

$$Fe(Ag, liq.) + 1/2\ O_2(g) + Cr_2O_3 = FeCr_2O_4 \qquad (16)$$

The iron content in the liquid silver phase was determined by inductively coupled plasma (ICP) spectroscopy after quenching and dissolution in nitric acid. An internal check on equilibrium was obtained by varying CO-CO_2 gas compositions at each temperature and demonstrating that a linear relationship existed between log iron concentration and log oxygen pressure with slope -1/2. This method is capable of very good accuracy. For example, one standard deviation calculated by comparing measured Gibbs energies for reaction (15) with the linear correlation versus temperature [51] gives ±1.75 kJ mol^{-1}. We note that the published value $\sigma = \pm 6.80$ kJ mol^{-1} [51] appears to be in error.

Some choices can also be made amongst the emf studies. As was the case for the Cr_2O_3 studies discussed above, the oxygen fugacity of reaction (15) is too low to permit a calcia-stabilized zirconia electrolyte to function solely as an ionic conductor. Analysis of more oxidizing reactions may not have been possible however, as the equivalent w**h**stite-bearing reaction:

$$\text{`FeO'} + Cr_2O_3 = FeCr_2O_4 \qquad (17)$$

is independent of oxygen fugacity (except as relates to the variable defect structure of the w**h**stite). This reaction is, therefore, not a suitable candidate for solid electrolyte studies. In the next most oxidizing reaction in this system:

$$Fe_3O_4 + Cr_2O_3 = FeCr_2O_4 + O_2 \qquad (18)$$

the iron oxide, magnetite, is also a spinel, and thus solid solutions between the two may form during the experiment, and the use of this reaction would also have been questionable. Finally, the reaction:

$$Fe_2O_3 + Cr_2O_3 = FeCr_2O_4 + O_2 \quad (19)$$

may have been usable, but the magnetite stability field will limit the upper thermal stability of the hematite - chromite assemblage. Regardless of the reasons for the choice of experimental reaction, however, the measured emf values from the studies of Tretjakow and Schmalzreid [25], Freuhan [53] and Snethlage and Klemm [54] are likely to be too small, the oxygen fugacities too high, and the magnitude of the Gibbs energies too small. Electrode polarization would have enhanced this effect. This is reflected in the relatively large, positive differences between their Gibbs energies and those reported by others using different emf methods (see Table 8).

Having explained the reasons for the largest discrepancies amongst several of the experimental data sets, causes for the remaining differences between the data of Katsura and Muan [50], Hino et al. [51], Rezukhina et al. [52], Jacob and Alcock [55], Zabievorota et al. [30] and Nagata and Murohashi [56] are uncertain. The reasons for the differences amongst the emf studies may include polarization effects or calibration of reference buffers, and uncertainties in composition and the ordering state of the spinel may also be involved. Barring the acquisition of additional, better constrained data, however, some decision must be made as to where to fix the Gibbs energy of reaction.

The results of Hino et al. [51] (-214.04 ±1.75 kJ mol^{-1}), Rezukhina et al. [52] (-213.36 ±0.29 kJ mol^{-1}), Jacob and Alcock [55] (-214.85 ±0.62 kJ mol^{-1}) and Zabeivorota et al. [30] (-214.38 ±0.42 kJ mol^{-1}) were chosen, somewhat arbitrarily at 1400 K, as the basis for determining the thermodynamic properties of $FeCr_2O_4$. These studies represented both gas mixing and emf methodologies and were considered to be the most reliable; the emf studies being conducted with three different electrolytes. In this manner, the high temperature Gibbs energy reference point for reaction (15) was selected as $\Delta_f G°$(1400 K) = -214.16 ±0.63 kJ mol^{-1}.

Downward thermodynamic extrapolation of Gibbs energies for reaction (15) from 1400 to 298.15 K using Eqs. (10, 11) required application of two different heat capacity curves for Fe to account for its structural transition at 1185 K, see Tables 5 and 6. In addition, two λ-transitions (at 1043 K in Fe and at 307 K in Cr_2O_3) also needed to be accounted for. Since the λ-transitions affect heat capacities over extended temperature intervals, it was necessary that the Maier-Kelley parameters selected for Fe and Cr_2O_3 represent $C_p^{lattice}$ rather than total C_p. This choice allowed (total) C_p to be correctly modeled by the sum of $C_p^{lattice}$ and C_p^{mag}, where the Inden model was used to quantify the latter. Table 6 summarizes Maier-Kelley parameters for the solids, i.e., for $C_p^{lattice}$, that are consistent with the phase transition parameters given in Table 7. The indicated thermodynamic extrapolation per Eq. (11) thus became

$$\Delta_f G°(1400\ K) = \Delta_f G°(298) - 1101.85\,\Delta_f S°(298) + 9215.34\ J\ mol^{-1}$$

The λ-transitions in Fe and Cr_2O_3 contributed 4492.49 and 1448.10 J mol^{-1}, respectively, to the final term in the above equation. Based on the entropy change for ferrous chromite

formation given in Table 5, it is calculated that $\Delta_f G°(298) = -289.44$ kJ mol^{-1} for reaction (15). Incorporating our previously-derived Gibbs energy for Cr_2O_3, we find $\Delta_f G°(298) = -1339.40$ kJ mol^{-1} for the $FeCr_2O_4$ formation reaction *from the elements*.

Included in Fig. 13 are the thermodynamically-extrapolated Gibbs energy changes for reaction (15) obtained by applying the above $\Delta_f G°(298)$ value and S°(298) from Table 5. Again, very close agreement is observed between thermodynamic extrapolation and the consensus, high-quality, literature results. The deviations, when viewed on an expanded scale (see Fig. 14), are seen to bracket the predictions to within ±2 kJ mol^{-1} throughout the entire temperature range. The large uncertainty ("3 J mol^{-1} K^{-1}) in the recently-measured value of S°(298) for $FeCr_2O_4$ [3] suggests, however, that our extrapolation could be improved by adjusting this parameter within its uncertainty limits. Given, however, that the initial calculations are already within the stated uncertainties in the measurements, such adjustments have not been adopted here. On the other hand, the outdated values for S°(298) in Barin [1] are seen to result in relatively poor $\Delta_f G°$ estimates for reaction (15).

4.3 Gibbs Energies of $ZnCr_2O_4$

The Gibbs energy of $ZnCr_2O$ is based on the single experimental study of Jacob [57] who measured the emfs of the reactions:

$$2\ Zn_{cu} + O_2 + 2\ Cr_2O_3 = 2\ ZnCr_2O_4 \qquad (20)$$

and

$$Zn_{cu} + 1/2\ O_2 = ZnO \qquad (21)$$

at 700-900°C, where Zn_{cu} is a 90% Cu -10 % Zn alloy used to keep the Zn from melting. Combining the results of these two measurements removes the uncertainties in the values of the Ni-NiO buffer used as the reference in each as well as those in the thermodynamic properties of Zn_{cu}. This yields the reaction:

$$ZnO + Cr_2O_3 = ZnCr_2O_4 \quad (22)$$

for which:

$$\Delta G^\circ = -62760 + 8.5772\ T\ (K, \pm 320\ J\ mol^{-1}) \quad (23)$$

Gibbs energies for $ZnCr_2O_4$ were, therefore, constrained to $\Delta G^\circ(1100\ K)$ determined using Eq. (23). Thermodynamic extrapolation from 1100 to 298.15 K using Eq. (11) and heat capacity correlations for $ZnCr_2O_4$ (Table 2), Cr_2O_3 (Table 2) and ZnO (Table 6) gives

$$\Delta_f G^\circ(1100\ K) = \Delta_f G^\circ(298) - 801.85\,\Delta_f S^\circ(298) + 5930.76\ J\ mol^{-1}$$

The above calculation also includes a contribution from the λ-transition in Cr_2O_3 (996.38 J mol^{-1}). Thus, $\Delta_f G^\circ(298)$ for reaction (22) extrapolates to -57.76 kJ mol^{-1}. Translating this result to zinc chromite formation *from the elements* using $\Delta_f G^\circ(298)$ values for Cr_2O_3 (derived herein) and ZnO (Table 6) gives $\Delta_f G^\circ(298) = -1428.35$ kJ mol^{-1}.

Fig. 15 shows the thermodynamically-extrapolated Gibbs energies as a function of temperature relative to the experimentally-fitted equation presented by Jacob [57]. The two curves are nearly coincident in the temperature interval 700-900°C, i.e., the range of the measurements; the maximum deviation being < 0.03 kJ mol^{-1}.

As noted above, the available data for reaction (22) severely constrain any possibility of varying the S°(298) or C_p data for Cr_2O_3 to better fit the experiments of Holzheid and O'Neill [2]. This is because increasing either value yields a poorer fit to reaction (22). While it seems likely that additional adjustments of the S°(298) and C_p data could further improve the fit, such changes are not warranted by either the precision or temperature range of the experiments of Jacob [57].

4.4 Gibbs Energies of $CoCr_2O_4$

Eight sets of experiments are available to constrain the Gibbs energy of $CoCr_2O_4$. These are summarized in Table 9, and shown in Fig. 16. The experiments of Schaefer [63] were based on the reaction:

$$Co + Cr_2O_3 + Cu_2O = 2Cu + CoCr_2O_4 \quad (24)$$

while the data of O'Neill and Pownceby [43] were used to calculate Gibbs energies for the buffer:

$$2\ Cu + 1/2\ O_2 = Cu_2O \quad (25)$$

and convert Schaefer's results to those for the reaction:

$$Co + 1/2\ O_2 + Cr_2O_3 = CoCr_2O_4 \quad (26)$$

Tretjakow and Schmalzreid [25] measured reaction (26) relative to air and provided a fitted equation for change in free energy for

$$CoO + Cr_2O_3 = CoCr_2O_4 \quad (27)$$

which was converted to values for reaction (26) using their data for the reaction:

$$Co + 1/2\ O_2 = CoO \quad (28)$$

Levitskii et al. [62] measured data for reaction (26) relative to the iron-wüstite buffer, but provide fitted equations only for the relative Gibbs energy and that of the reaction:

$$CoO + Fe = Co + FeO \quad (29)$$

which together yield reaction (27). This was converted to values for reaction (26) using the data of O'Neill and Pownceby [43].

Three of the four gas mixing studies studied the reaction:

$$Co + Cr_2O_3 + CO_2 = CO + CoCr_2O_4 \quad (30)$$

As noted previously, the data of Kunnmann et al. [49] are suspect as they are unreversed and generally have very large CO/CO_2 ratios (i. e., > 10). Closer examination of their results, however, reveals that the lowest CO/CO_2 ratios (< 10 at the highest temperatures) appear to have a different temperature dependency than the ratios at the lowest temperatures. Since the high temperature results of Kunnmann et al. are also in relatively good agreement with the results of the other gas mixing studies, only the data of Kunnmann et al. recorded below 1250 K have been ignored. The datum of Aukrust and Muan [58] appears to be reversed, and the equilibrium for reaction (27) has been reported as $\Delta G°(1623\ K) = -46.86 \pm 2.51$ kJ mol^{-1}. Addition of the equilibrium for reaction (28), as recommended by O'Neill and Pownceby [43], gives $\Delta_f G°(1623\ K) = -166.11$ kJ mol^{-1} for reaction (26). In a similar manner, the results of Jacob and Fitzner [60] and Koc and Timucin [61] for reaction (27) were converted to free energy changes for reaction (26) by adding the equilibrium for reaction (28) to give $\Delta_f G°(1373\ K) = -186.79$ kJ mol^{-1} and $\Delta_f G°(1573\ K) = -160.55$ kJ mol^{-1}, respectively.

Due to good temperature overlap between five of the eight investigations, 1373 K was selected as the common reference point at which $\Delta_f G°$(T) for reaction (26) was fixed. Unlike the data for $FeCr_2O_4$, the solid electrolyte chosen cannot be used to select among the various emf studies. This is because the fO_2 of the reaction is higher than that of reaction (15) used for the $FeCr_2O_4$ experiments (-17.3 at 1200 K as opposed to -20.0), and both types of solid electrolytes should act as purely ionic conductors in this range. Therefore, the thermodynamic extrapolation of Eq. (11) was initiated by defining $\Delta_f G°$(1373 K) from the average of five independent determinations: -181.42 ±1.05 kJ mol^{-1} [49] and -183.51 ±1.26 kJ mol^{-1} [59] based on gas mixing studies, and -190.07 ±0.19 kJ mol^{-1} [62], -184.85 ±0.39 kJ mol^{-1} [25] and -186.79 kJ mol^{-1} [60] based on emf measurements. The values attributed to Levitskii et al. [62] and Schaefer [63] represent revised values calculated herein by applying the recent results of O'Neill and Pownceby [43] based on updated Gibbs energies for the iron-wüstite and Cu-Cu_2O buffers. The reference Gibbs energy determined in this manner is $\Delta_f G°$(1373 K) = -185.33 "2.95 kJ mol^{-1}.

Thermodynamic extrapolation from the above high temperature reference point to 298.15 K was conducted using Eq. (11) with heat capacity correlations for $CoCr_2O_4$, Cr_2O_3, Co and O_2 taken from Tables 2 and 6:

$$\Delta_f G°(1373\ K) = \Delta_f G°(298) - 1074.85\,\Delta_f S°(298) + 5523.60\ J\ mol^{-1}$$

The λ-transitions in Co and Cr_2O_3 contributed 1664.15 and 1407.45 J mol^{-1}, respectively, to the final term in the above equation. Based on $\Delta_f S°(298) = -79.955\ J\ mol^{-1}\ K^{-1}$ for reaction (26) as determined from the standard molar entropies given in Tables 3 and 6, it is found that $\Delta_f G°(298) = -276.79$ kJ mol^{-1}. Finally, combining the equilibria for

reactions (26) and (14) yields $\Delta_f G°(298)$ = -1326.75 kJ mol^{-1} for cobalt chromite formation *from the elements*.

Figure 16 plots the thermodynamically-extrapolated Gibbs energies for $CoCr_2O_4$ formation via Eq. (26), calculated using the above $\Delta_f G°(298)$ value and S°(298) from Table 5, and compares them to the experimental database. The deviations, when viewed on an expanded scale (see Fig. 17), are in good agreement with the consensus, higher-quality, literature results. For example, deviations relative to the database consisting of the above five 'consensus' $\Delta_f G°(1373\ K)$ results, in addition to the results of Aukrust and Muan [58], are seen to bracket the predictions to within ±3 kJ mol^{-1} throughout the entire temperature range. On the other hand, the results of Schaefer [63] and Koc and Timucin [61] are seen to be outliers. Also shown in Fig. 17 are deviations relative to predictions for Eq. (26) based on properties compiled by Barin [1]: $\Delta_f G°(298)$ = -271.71 kJ mol^{-1} and $\Delta_f S°(298)$ = -87.46 J mol^{-1} K^{-1}. The resulting Gibbs energies for $CoCr_2O_4$ formation are seen to be 10 to 15 kJ mol^{-1} more positive than the present extrapolation; the source of the deviation lying in neglect of the entropy contributed by the magnetic transition in $CoCr_2O_4$ at 24 K.

5. DISCUSSION

5.1 Thermodynamic Properties of Cr_2O_3

The enthalpy of formation of Cr_2O_3 at 298.15 K derived in this work, $\Delta_f H°(298)$ = -1131.21 kJ mol^{-1}, is less negative than the value adopted by Chase [40] by 3.49 kJ mol^{-1} (i.e., -1134.70 kJ mol^{-1}) where his estimate was based on an average of the results of Mah

[34] and Golutvin and Chin'k'uei [35], obtained by ambient temperature calorimetry, and Jeannin et al. [22], Novokhatskii and Lenev [23], and Mazandarany and Pehlke [28], obtained by extrapolation of high temperature measurements. The lack of reproducibility among the 1 atm., 25°C experimental results for $\Delta_f H°(298)$ argues against their adoption as reference values.

Our reference point Gibbs energy for Cr_2O_3 (at elevated temperature) includes additional, recent results of Jacob [29], Zabeivorota et al. [30] and Holzheid and O'Neill [2] in the averaging process and considered only high temperature results. We believe that this change is justified by recent advances in high temperature emf measurement techniques.

Sufficient heat capacity data for Cr_2O_3 are now available to permit definition of the θ-transition observed at ~307 K. Thermodynamic changes associated with the magnetic transition, determined from the fitted Inden model parameters, are

$$\Delta S^{mag} / R = 2\left[K^{-}C' + K^{+}D'\right] = 1.494 \tag{31}$$

and

$$\Delta H^{mag} / R = -2T_c\left[-K^{-}A' + K^{+}B'\right] = 412.518 \tag{32}$$

Since magnetic entropy may be defined in terms of the mean atomic moment, β (in Bohr magnetons per atom), as

$$\Delta S^{mag} / R = \ln\left(\beta + 1\right) \tag{33}$$

it is found that β = 0.83. It is noted that these calculations represent only a portion of the thermodynamic changes associated with the magnetic transition in Cr_2O_3 because the

fitted $C_P^{baseline}$ contribution actually represents the sum of two effects: (1) the true lattice vibrational contribution and (2) the remaining portion of the magnetic contribution (i.e., the long-range ordering phenomenon). Only at temperatures above T_N do the fitted heat capacities represent the lattice vibrational contribution. The existence of this combination below T_N provides an explanation for the sign difference in the Maier-Kelley parameters for Cr_2O_3 relative to those for the chromites (where the M-K parameters represent the true lattice vibrational contribution at all temperatures fitted). Further work, similar to that used to interpret heat capacity behavior of the transition metal ferrites [64], is required to extract thermodynamic changes associated with the loss of magnetic ordering in Cr_2O_3 and to provide a C_P fit that is valid down to absolute zero.

Recent heat capacity measurements of metallic chromium [65] have revealed a 8-type anomaly around 311 K due to a magnetic transition. The thermodynamic changes associated with the transition, however, are much smaller than those found for Cr_2O_3: ΔS^{mag} = 66.2 mJ mol^{-1} K^{-1} and ΔH^{mag} = 18.6 J mol^{-1} (see Table 7). The effect on Gibbs energy of Cr_2O_3 caused by accounting for the 8-transition in Cr was to decrease $\Delta_f G°(298)$ by < 0.04 kJ mol^{-1}. This change is insignificant compared to the correction required for including the 8-transition in Cr_2O_3, i. e., 1.00 kJ mol^{-1}.

5.2 Comparison of High-Temperature Heat Capacity Results

Fig. 18 compares the high-temperature C_p results for the family of transition metal chromites MCr_2O_4 (M = Fe, Ni, Co, Zn). In the temperature range shown, heat capacities are expected to be dominated by lattice vibrational effects. In order to emphasize this

behavior in Fig. 18, all C_P values were made dimensionless by dividing by $3nR$, where $n = 7$ for the MCr_2O_4 and MFe_2O_4 spinels and $n = 5$ for Cr_2O_3. The order Ni > Co > Fe > Zn appears to exist, although the spread between high and low values (~ 7%) borders on statistical significance.

A similar order exists for the family of transition metal ferrites (MFe_2O_4), based on our previous work [64], see Fig. 18. Although the ferrites undergo a magnetic transition around 860 K, which would be expected to increase heat capacities, the temperature range selected for comparison is sufficiently high so that the measured heat capacities represent a purely lattice vibrational effect. It is believed that the greater heat capacities of the ferrites may be due to the inverse spinel configuration of the ferrites versus the normal spinel configuration of the chromites, rather than a vibrational difference between the Fe^{3+} and Cr^{3+} ions.

It is noteworthy that a second anomaly appears in the heat capacity curves for the family of chromites in the vicinity of 70-90 K that is similar to one found previously for the family of ferrites; see Table 11. In the latter cases, we found that the anomaly resembled a Schottky anomaly and was included in the contribution to $C_P^{lattice}$ rather than C_P^{mag} [64]. Although this anomaly has been associated with the relaxation of acoustic lattice modes [67] or transitions by the Fe^{3+} ion between two equivalent potential minima within the octahedral site [68], future work is required to develop these hypotheses.

6. SUMMARY/CONCLUSIONS

High temperature heat capacity measurements were obtained for Cr_2O_3, $FeCr_2O_4$, $ZnCr_2O_4$ and $CoCr_2O_4$ using a differential scanning calorimeter. These data were combined with previously-available, overlapping heat capacity data at temperatures up to 400 K and fitted to 5-parameter Maier-Kelley $C_p(T)$ equations. Expressions for molar entropy were then derived by suitable integration of the Maier-Kelley equations in combination with recent S°(298) evaluations. The latter analysis was affected by magnetic transitions which created anomalies in the heat capacity curves at low temperature: 11.5 K ($ZnCr_2O_4$), 24 K ($CoCr_2O_4$) and 36.5 K ($FeCr_2O_4$) and by additional, Schottky-type anomalies at 95 K ($CoCr_2O_4$) and 69 K ($FeCr_2O_4$).

The availability of high temperature heat capacities (and entropies) permitted thermodynamic extrapolations to be performed on Gibbs energies of these oxides obtained from equilibrium measurements at high temperature. A database was constructed from available literature and critically evaluated to provide reference free energies for the following reactions:

(1) $Cr + 3/2O_2 = Cr_2O_3$ $\Delta G°(1100\ K) = -840.58 \pm 1.48\ kJ\ mol^{-1}$

(2) $Fe + 1/2O_2 + Cr_2O_3 = FeCr_2O_4$ $\Delta G°(1400\ K) = -214.16 \pm 0.54\ kJ\ mol^{-1}$

(3) $ZnO + Cr_2O_3 = ZnCr_2O_4$ $\Delta G°(1100\ K) = -53.325 \pm 0.32\ kJ\ mol^{-1}$

(4) $Co + 1/2O_2 + Cr_2O_3 = CoCr_2O_4$ $\Delta G°(1373\ K) = -185.33 \pm 2.95\ kJ\ mol^{-1}$

Extrapolation of the above equilibria to 298.15 K was performed using available heat capacity correlations for the reactants, after accounting for λ-type thermal anomalies caused by magnetic transitions at the following temperatures: 311 K (Cr), 307 K (Cr_2O_3), 1043 K (Fe) and 1396 K (Co). In this manner, it was found that $\Delta_f G°(298) = -1049.96$, -

1339.40, -1428.35 and -1326.75 kJ mol^{-1} for Cr_2O_3, $FeCr_2O_4$, $ZnCr_2O_4$ and $CoCr_2O_4$, respectively.

ACKNOWLEDGEMENT

The authors are grateful to Dr. A. R. Gaddipati for synthesis of Cr_2O_3 and the chromites used in this study. The low temperature heat capacity measurements of $CoCr_2O_4$ were performed by Drs. Rebecca Stevens, Brian F. Woodfield and Juliana Boerio-Goates at Brigham Young University.

REFERENCES

[1] I. Barin, Thermochemical Data of Pure Substances. VCH Verlagsgesellschaft mbH, D-6940 Weinheim, 1993.

[2] A. Holzheid, H. St. C. O'Neill, The Cr-Cr_2O_3 oxygen buffer and the free energy of formation of Cr_2O_3 from high-temperature electrochemical measurements. Geochim. Cosmochim. Acta. **59** (1995) 475-479.

[3] S. Klemme, H. St. C. O'Neill, W. Schnelle, E. Gmelin, The heat capacity of $MgCr_2O_4$, $FeCr_2O_4$ and Cr_2O_3 at low temperatures and derived thermodynamic properties. Amer. Mineral. **85** (2000) 1686-1693.

[4] G. Shirane, D. Cox, S. Pickard, Magnetic structures in $FeCr_2S_4$ and $FeCr_2O_4$. J. Appl. Phys. **35** (1964) 954-955.

[5] S. Klemme, J. C. van Miltenburg, Thermodynamic properties of nickel chromite ($NiCr_2O_4$) based on adiabatic calorimetry at low temperatures. Phys. Chem. Minerals **29** (2002) 663-667.

[6] S. Klemme, J. van Miltenburg, The entropy of zinc chromite ($ZnCr_2O_4$). Miner. Mag. **68** (2004) 515-522.

[7] R. Stevens, B. F. Woodfield, J. Boerio-Goates, Heat capacity measurements of $CoCr_2O_4$(cr) from $0.5 < T/K < 400$ and thermodynamic functions from $0 < T/K < 400$. unpublished data.

[8] D. J. Wesolowski, S. E. Ziemniak, L. M. Anovitz, M. L. Machesky, P. Benezeth, D. A. Palmer, in: D. A. Palmer, R. Fernandez-Prini, A. H. Harvey (Eds.), Aqueous Systems at Elevated Temperatures and Pressures, Elsevier Ltd, London, 2004, pp. 493-595.

[9] S. E. Ziemniak, M. E. Jones, K. E. S. Combs, Solubility and phase behavior of Cr(III) oxides in alkaline media at elevated temperatures, J. Solution Chem. **27** (1998) 33-65.

[10] R. A. Robie, B. S. Hemingway, Thermodynamic properties of minerals and related substances at 298.15 K and 1 bar (10^5 pascals) pressure and at higher temperatures. US Geol. Surv. Bull. 2131 (1995).

[11] R. H. Bruce, D. S. Cannell, Specific heat of Cr_2O_3 near the N**J**el temperature. Phys. Rev. B **15** (1977) 4451-59.

[12] D. de Fontaine, S. G. Fries, G. Inden, P. Miodownik, R. Schmid-Fetzer, S.-L. Chen, Thermodynamic models and data for pure elements and other endmembers of solutions; Group 4: λ-transitions. Calphad **19** (1995) 499-536.

[13] A. T. Dinsdale, SGTE data for pure elements. Calphad **15** (1991) 317-425.

[14] B. Sundman, An assessment of the Fe-O system. J. Phase Equil. **12** (1991) 127-40.

[15] B. F. Naylor, High-temperature heat contents of ferrous and magnesium chromites. Ind. Eng. Chem. **36** (1944) 933-934.

[16] JCPDS Powder Diffraction File, International Centre for Diffraction Data, Swarthmore, PA, 1989

[17] C. H. Shomate, Ferrous and magnesium chromites. Specific heats at low temperatures. Ind. Eng. Chem. **36**, (1944) 910-912.

[18] A. S. Russell, Messung von spezifischen W@rmen bei tiefen Temperaturen. Z. Physik. **13** (1912) 59.

[19] I. Ya. Granat, Reduction of chromium oxide. Metallurg. **11** (1936) (No. 10) 35-41

[20] G. Grube, M. Flad, The reduction equilibrium of chromic oxide. Z. Electrochem. **45** (1939) 835-837.

[21] J. N. Ramsey, D. Caplan, A. A. Burr, Thermodynamics of the oxidation of chromium. J. Electrochem. Soc., **103** (1956) 135-138.

[22] Y. Jeannin, C. Mannerskantz, F. E. Richardson, Activities in iron-chromium alloys. Trans. Metall. Soc. AIME **227** (1963) 300-305.

[23 I. A. Novokhatskii, L. M. Lenev, Thermodynamic properties of Cr_2O_3 and $FeCr_2O_4$ at high temperatures. Russ. J. Inorg. Chem. **11** (1966) 1078-1081.

[24] N. Y. Toker, L. S. Darken, A. Muan, Equilibrium phase relations and thermodynamics of the Cr-O system in the temperature range of 1500 to 1825°C. Metall. Trans. **22B** (1991) 225-232.

[25] J. D. Tretjakow, H. Schmalzreid, Zur Thermodynamik von Spinellphasen (Chromite, Ferrite Aluminate). Ber. Bunsenges. Phys. Chem. **69** (1965) 396-402.

[26] L. A. Pugliese, G. R. Fitterer, Activities and phase boundaries in the Cr-Ni system using a solid electrolyte technique. Metall. Trans. **1** (1970) 1997-2002.

[27] K. Suzuki, K. Sambongo, High-temperature thermodynamic properties in Ti-O systems. Tetsu To Hagane **58** (1972) 1579-1602.

[28] F. N. Mazandarany, R. D. Pehlke, Standard free energy of formation of Cr_2O_3, J. Electrochem. Soc. **121** (1974) 711-714.

[29] K. T. Jacob, Potentiometric determination of the Gibbs free energy of formation of cadmium and magnesium chromites. J. Electrochem. Soc. **124** (1977) 1827-1831.

[30] N. S. Zabeivorota, A. A. Likasov, G. G. Mikailov, Free energy of the formation reaction of $FeCr_2O_4$. Izv. Akad. Nauk SSSR Neorg. Mater. **16** (1980) 181-3.

[31] W. G. Mixter, Unstable chromium sesquioxide, and corrections of previous work on the heat effect of chromium and aluminum sesquioxides in fusions with sodium peroxide. Amer. J. Sci. **39** (1915) 295-299.

[32] W. A. Roth, G. Becker, Thermochemical revisions. Z. Physik. Chem. **A145** (1929) 461- 469.

[33] W. A. Roth, A. Wolf, Die Bildungsw@rme von Chromioxyd. Z. Electrochem. **46** (1940) 45-46.

[34] A. D. Mah, Heats of formation of chromium oxide and cadmium oxide from combustion calorimetry. J. Amer. Chem. Soc. 7**6** (1954) 3363-3365.

[35] Yu. M. Golutvin, L. Chin'k'uei, Heats of formation, heat contents and heat capacities of chromium silicides. Russ. J. Phys. Chem. **35** (1961) 62-67.

[36] C. T. Anderson, The heat of chromium, chromic oxide, chromous chloride, and chromic chloride at low temperatures. J. Amer. Chem. Soc. **59** (1937) 488-491.

[37] J. Volger, Anomalous specific heat of chromium oxide (Cr_2O_3) at the antiferromagnetic Curie temperature. Nature **170** (1952) 1027.

[38] P. N. Laschschenko, D. I. Komanskii, The relationship between the various forms of calcium sulfate at high temperatures. J. Russ. Phys. Chem. Soc. **60** (1928) 579.

[39] G. E. Moore, K. K. Kelley, High-temperature heat contents of the chromium carbides and of chromic oxide. U. S. Bureau of Mines Technical Report 662 (1944) 43pp.

[40] M. W. Chase, NIST-JANAF Thermochemical Tables, Fourth Edition. J. Phys. Chem. Ref. Data (1998) Monograph No. 9.

[41] W. L. Worrell, Oxide solid electrolytes. in: Solid Electrolytes, S. Geller (Ed.), Topics in Applied Physics **21** (1977) 143-168. Springer-Verlag, Berlin.

[42] L. N. Anovitz, Electrochemical determination of the Gibbs energies of rock-forming minerals. U. S. Department of Energy Report DOE/ER/14115 (1995)

[43] H. St. C. O'Neill, M. I. Pownceby, Thermodynamic data from redox reactions at high temperatures. I. An experimental and theoretical assessment of the electrochemical method using stabilized zirconia electrolytes, with revised values for the Fe -"FeO", Co-

CoO, Ni -NiO and Cu-Cu_2O oxygen buffers, and new data for the W -WO_2 buffer. Contrib. Mineral. Petrol. **114** (1993) 296 -314.

[44] O. Knacke, O. Kubaschewski, K. Hesselmann, Thermodynamic Properties of Inorganic Substances, Springer, Berlin, 1991.

[45] H. Watanabe, Thermal constants for Ni, NiO, MgO, MnO and CoO at low temperatures. Thermochim. Acta, **218** (1993) 365-372.

[46] F. J. Romero, J. Jimenez, J. Del Cerro, Calorimetric investigation on the paramagnetic-antiferromagnetic phase transition in CoO. J. Magnetism and Magnetic Materials **280** (2004) 257-263.

[47] F. S. Boericke, W. M. Bangert, Equilibrium in the reduction of ferrous chromite by hydrogen and energy requirements in the selective reduction of iron in chromite. USBM Rept. Inv. 3813 (1945) 19 pp.

[48] H.-M. Chen, J. Chipman, The chromium-oxygen equilibrium in liquid iron. Trans. Amer. Soc. Metals **38** (1947) 70-116.

[49] W. Kunnmann, D. B. Rogers, A. Wold, The use of CO-CO_2 atmospheres for the preparation and free energy determinations of several oxide systems. J. Phys. Chem. Solids **24** (1963) 1535-1538.

[50] T. Katsura, A. Muan, Experimental study of equilibria in the system FeO-Fe_2O_3-Cr_2O_3 at 1300°C. Trans. Met. Soc. AIME **230** (1964) 77-84.

[51] M. Hino, K. Higuchi,T. Nagasaka, S. Ban-ya, Phase equilibria and activities of the constituents in FeO-Cr_2O_3 - MgO-Cr_2O_3 spinel solid solution saturated with Cr_2O_3. ISIJ International **34** (1994) 739-745.

[52] T. N. Rezukhina, V. A. Levitskii, B. A. Istomin, Thermodynamic properties of iron chromite from electrochemical measurements. Electrochimiya **1** (1965) 467-471.

[53] R. J. Freuhan, Activities in the liquid Fe-Cr-O system. Trans Metall. Soc. AIME **245** (1969) 1215-1218.

[54] R. Snethlage, D. D. Klemm, Das System Fe-Cr-O bei 1000, 1095 und 1200° C. N. Jb. Miner. Abh. **125** (1975) 227-242.

[55] K. T. Jacob, C. B. Alcock, The oxygen potential of the systems Fe + $FeCr_2O_4$ + Cr_2O_3 and Fe + FeV_2O_4 + V_2O_3 in the temperature range 750-1600°C. Metall. Trans. **6B** (1975) 215-221.

[56] K. Nagata, R. Murohashi, The standard free energy of $Fe_{1+x}Cr_{2-x}O_4$ spinel equilibrated with iron, Zairyo to Purosesu (CAMP-ISIJ) **3** (1990) 940.

[57] K. T. Jacob, Gibbs free energies of formation of $ZnAl_2O_4$ and $ZnCr_2O_4$. Thermochim. Acta **15**, (1976) 79-87.

[58] E. Aukrust, A. Muan, The stabilities of $CoOCAl_2O_3$, $CoOCCr_2O_3$, and $2CoOCSiO_2$. J. Amer. Ceram. Soc., **46** (1963) 358.

[59] L. N. Lenev, I. A. Novokhatskii, Thermodynamic properties of cobalt and nickel chromites. Russ. J. Phys. Chem. **40** (1966) 1097-1099.

[60] K. T. Jacob, K. Fitzner, Ion-exchange equilibria between (Mn, Co)O solid solution and (Mn, Co)Cr_2O_4 and (Mn, Co)Al_2O_4 spinel solid solutions at 1100°C. J. Mater. Sci. **12**, (1977) 481-488.

[61} N. Koc, M. Timucin, Activity-composition relations in $MnCr_2O_4$-$CoCr_2O_4$ solid solutions and stabilities of $MnCr_2O_4$ and $CoCr_2O_4$ at 1300°C. J. Amer. Ceram. Soc. **88** (2005) 2578-2585.

[62] V. A. Levitskii, T. N. Rezukhina, A. S. Guzei, The thermodynamic properties of cobalt chromite from electrochemical measurements at 1270-1490°K. Soviet Electrochem. **1** (1965) 200-202.

[63] S. C. Schaefer, Electrochemical determination of thermodynamic properties of $NiCr_2O_4$ and $CoCr_2O_4$. USBM Rept. of Invest. 9043 (1986) 11pp.

[64] S. E. Ziemniak, L. M. Anovitz, R. A. Castelli, W. D. Porter, Magnetic contribution to heat capacity and entropy of nickel ferrite ($NiFe_2O_4$). J. Phys. Chem. Solids **67** (2006) in press.

[65] I. S. Williams, E. S. R. Gopal, R. Street, The specific heat of strained and annealed chromium. J. Phys. F **9** (1979) 431-45.

[66] D. M. Chizhikov, B. S. Gol'dman, E. K. Kazenas, Heat capacities of nickel aluminate, titanate and chromite at high temperatures. Russ. J. Phys. Chem. **49** (1975) 283.

[67] N. W. Grimes, On the specific heat of compounds with spinel structure. I. The ferrites, Proc. R. Soc. Lond. A. **338** (1974) 209-221.

[68] N. W. Grimes, On the specific heat of compounds with spinel structure. II. Zinc ferrite, a paramagnetic compound with magnetic ion occupying the octahedral site. Proc. R. Soc. London A **338** (1974) 223-233.

Table 1

Crystallographic Features of the Metal Oxides Tested

Oxide	Crystal Symmetry	Lattice Parameter(s)
Cr_2O_3	rhombohedral	a_o = 4.9589 (3) D
		c_o = 13.5930 (9) D
$FeCr_2O_4$	cubic	a_o = 8.3780(5) D
$ZnCr_2O_4$	cubic	a_o = 8.3276(1) D
$CoCr_2O_4$	cubic	a_o = 8.3320(1) D

Table 2

Maier-Kelley Parameters Used in Eq. (1) Heat Capacity Correlations

Compound	A	B	C	D	E	Range of Validity, K
Cr_2O_3[a]	146.822	$-3.86976\ 10^{-3}$	$6.97636\ 10^{-7}$	-660.534	$-5.23849\ 10^{5}$	250 - 1373
$FeCr_2O_4$	157.019	$2.92977\ 10^{-2}$	$-7.39320\ 10^{-6}$	-206.323	$-1.71417\ 10^{6}$	200 - 1473
$CoCr_2O_4$	64.570	$8.77263\ 10^{-2}$	$-1.92883\ 10^{-5}$	1481.276	$-3.96915\ 10^{6}$	250 - 1657
$ZnCr_2O_4$	173.791	$9.40473\ 10^{-3}$	$-1.42748\ 10^{-6}$	-305.919	$-2.68034\ 10^{6}$	250 - 1373

[a] Does not include contribution from antiferromagnetic-paramagnetic transition at 306.99 K ; need to add Inden model Eqs. (5, 6): m = 7.280 ($K^- = 1.454$) and n = 16.948 ($K^+ = 1.060$), see text.

Table 3

Reference Point Entropy Integral (F) and S°(298) Values for Eq. (3)

Oxide	S°(298) J $mol^{-1}K^{-1}$	Ref.	F J $mol^{-1}K^{-1}$
Cr_2O_3[a]	82.3"0.3	Klemme et al. [3]	914.86
$FeCr_2O_4$	152.2"3.0	Klemme et al. [3]	936.58
$ZnCr_2O_4$	127.4"0.3	Klemme and van Miltenburg [6]	1043.44
$CoCr_2O_4$	134.96"0.3	Boerio-Goates et al.[7]	243.94

[a] Application to Cr_2O_3 requires addition of 1.506 J $mol^{-1}K^{-1}$ to account for modification of Eqs. (2, 3) caused by existence of a magnetic transition at 306.98 K, see text.

Table 4

Summary of Literature on the Thermochemical Properties of Cr_2O_3

Reference	Technique	Temp. Range	$\Delta_f G°(1100\ K)$[a] kJ mol^{-1}	Comments
Granat [14] (1936)	gas mixing - H_2-H_2O	1273 – 1773 K		disagree with Jeannin
Grube and Flad [20] (1939)	gas mixing - H_2-H_2O	1168 – 1275 K		disagree with Jeannin
Ramsey et al. [21] (1956)	gas mixing - H_2-H_2O	871 - 1427 K	(??)	
Jeannin et al. [22] (1963)	gas mixing - H_2-H_2O	1313 - 1573 K	-839.96±1.26	
Novokhatskii and Lenev[23] (1966)	gas mixing - H_2-H_2O	1493 - 1893 K	-848.88	linear extrapolation
Toker et al. [24] (1991)	gas mixing - H_2-CO_2	1773 - 1923 K		
Tretjakow and Schmalzreid [25] (1965)	emf - CDZ - air ref	1000 – 1500 K	-827.93	disregard, fO_2 too low for CDZ
Pugliese and Fitterer [26] (1970)	emf - CDZ			disregard, fO_2 too low for CDZ
Suzuki and Sambongi [27] (1972)	emf - YDT - Fe-FeO ref	1173 – 1823 K	-831.92±0.63	also Mn-MnO and Ta-Ta_2O_5 refs
Mazandarany and Pehlke [28] (1974)	emf - YDT - Co-CoO ref	1150 - 1540 K	-840.32±1.46	also Mn-MnO ref
Jacob [29] (1977)	emf - YDT - Co-CoO ref	800 - 1200 K	-840.56±0.90	
Zabeivorota et al. [30] (1980)	emf - YDZ - Mo-MoO_2 ref	1000 - 1973 K	-843.26±3.14	also Fe-V_2O_3-FeV_2O_4 ref
Holzheid and O'Neill [2] (1995)	emf - YDT - Fe-FeO ref	900 - 1350 K	-838.78±0.26	
Mixter [31] (1915)	Cr_2O_3 calorimetry	298.15 K	-1120.48	$\Delta_f H$ (298)
Roth and Becker [32] (1929)	Cr_2O_3 calorimetry	298.15 K	-1208.76	$\Delta_f H$ (298), well out of range of others
Roth and Wolf [33] (1940)	Cr_2O_3 calorimetry	298.15 K	-1125.08	$\Delta_f H$ (298)
Mah [34] (1954)	Cr_2O_3 calorimetry	298.15 K	-1140.56	$\Delta_f H$ (298)
Golutvin and Chin'k'uei [35] (1961)	Cr_2O_3 calorimetry	298.15 K	-1133.86	$\Delta_f H$ (298)
Russell [18] (1912)	Cp	137 - 299 K		
Anderson [36] (1937)	Cp	56 - 336 K		
Volger[37] (1952)	Cp	100 - 350 K		
Bruce and Cannell [11] (1977)	Cp	290.68 - 323.43 K		
Klemme et al. [3] (2000)	Cp	1.48 - 340 K		$S°(298) = 82.8±0.8$ J mol^{-1} K^{-1}
Laschschenko and Komanskii [38] (1928)	enthalpy	288 - 1428 K		
Moore and Kelley [39] (1944)	enthalpy	298 - 1774 K		

[a] Gibbs energy change for reaction (14)

Table 5

Thermodynamic coefficients in Eq. (11) for Gibbs energies of formation of Cr_2O_3, $FeCr_2O_4$, $ZnCr_2O_4$ and $CoCr_2O_4$ via the reaction indicated

T range K	ΔS°(298) J mol^{-1} K^{-1}	a	b	c	d	e	f (298) J mol^{-1} K^{-1}	g (298) J mol^{-1}	) G°(ref)[a] kJ mol^{-1}
				$2\ Cr + 1.5\ O_2 = Cr_2O_3$					
298-2180	-272.511	49.275	-0.00601	-15.4989E-06	-660.534	3.09151E+05	353.036	-9560.6	-840.58
				$Fe + 1/2O_2 + Cr_2O_3 = FeCr_2O_4$					
298-1185	-59.955	-27.894	0.02113	-7.9344E-06	454.211	-9.43604E+05	-200.285	11403.1	-214.16
1185-1667		-29.044	0.02241	-7.9344E-06	454.211	-9.43604E+05	n.a.	n.a.	
				$Co + 1/2O_2 + Cr_2O_3 = CoCr_2O_4$					
298-1768	-79.955	-121.915	0.08305	-20.5169E-06	2141.81	-3.20825E+06	-900.809	51886.8	-185.33
				$ZnO + Cr_2O_3 = ZnCr_2O_4$					
298-2000	1.87	-18.369	0.00598	-2.1251E-06	354.615	-1.58349E+06	-135.137	12327.9	-53.32

[a] Reference temperatures for the Cr_2O_3, $FeCr_2O_4$, $CoCr_2O_4$ and $ZnCr_2O_4$ formation reactions are 1100, 1400, 1373 and 1100 K, respectively.

Table 6

Maier-Kelley parameters and thermodynamic properties for reactant phases of interest[a]

	S°(298) J mol^{-1} K^{-1}	A	B	C	D	E	F [b] J mol^{-1} K^{-1}	$\Delta_f G°(298)$ J mol^{-1}
Cr(bcc)	23.543	26.908	-3.7886E-03	8.86326E-06	0	-2.7850E+05	154.142	0
O_2 [c]	205.15	29.154	6.48E-03	-1.02E-06	0	-1.84E+05	169.028	0
CoO [c]	52.80	45.258	1.069E-02	0	0	6.02E+05	257.664	-214190.
ZnO [c]	43.20	45.338	7.29E-03	0	0	-5.73E+05	263.714	-320636.
Zn <692.66 K	41.63	0	2.80E-02	-5.41E-06	349.81	-2.46E+05	-31.024	0
Co(hcp/fcc)	30.040	25.0861	5.30948E-03	1.04088E-6	0	-1.45054E+5	145.376	0
Fe(bcc)	27.280	23.5143	8.79504E-03	3.535614E-7	0	-1.54717E+5	137.483	0
Fe(fcc)	n. a.	24.6643	7.51504E-03	3.535614E-7	0	-1.54717E+5	n. a.	0

[a] Data taken from Dinsdale [13]. [b] Free energy extrapolations via Eqs. (10, 11) may require modification for inclusion of thermal anomalies due to structural and magnetic ordering transitions given in Table 7. [c] Heat capacity taken from Knacke et al. [44].

Table 7

Thermodynamic Changes Associated with Solid Phase Structural and Magnetic Ordering Transitions[a]

Transition	Temp. K	$\Delta_{trans}H°$ J mol^{-1}	$\Delta_{trans}S°$ J mol^{-1} K^{-1}	$\Delta_{trans}C_p$ J mol^{-1} K^{-1}	K^{-} [b]	K^{+} [b]	Notes
Cr(λ, bcc)	311.5	18.62 [b]	0.06625 [b]	[b]	0.007325	0.005096	β = 0.008
Co(hcp → fcc)	694.99	427.59	0.6153	0	n. a.	n. a.	
Co(λ, fcc)	1396.	8500.34 [b]	7.104 [b]	[b]	0.8945	0.3648	β = 1.35
Fe(λ, bcc)	1043.	9150.12 [b]	9.723 [b]	[b]	1.073	0.7504	β = 2.22
Fe(bcc → fcc)	1184.8	1012.87	0.8549	-7.682	n. a.	n. a.	
Fe(fcc → bcc)	1667.5	825.78	0.4953	2.183	n. a.	n. a.	
CoO(λ, fcc) [c]	288.95	1686.35 [b]	6.820 [b]	[b]	0.8629	0.3434	β = 1.27

[a] Data taken from Dinsdale [13]. [b] Thermodynamic changes calculated using Inden model with m = 3, n = 5; indicated enthalpy and entropy changes are for ΔH^{mag} and ΔS^{mag}. [c] Data of Watanabe [45] fitted to Inden model, constraining lattice contribution to Romero et al. [46].

Table 8

Experimental Studies on the Stability of $FeCr_2O_4$

Reference	Technique	Temp. Range	$\Delta_f G°$(1400 K)[a] kJ mol^{-1}	Comments
Boericke and Bangert [47] (1945)	gas mixing - H_2-H_2O	(??)		
Chen and Chipman [48] (1947)	gas mixing - H_2-H_2O	1868 K		
Kunnmann et al. [49] (1963)	gas mixing - CO-CO_2	1073 - 1380 K	-191.95	$\Delta_f G$ > 22 kJ mol^{-1} larger than Jacob and Alcock [55] (1975) - not on figure
Katsura and Muan [50] (1964)	gas mixing - H_2-CO_2	1300°C		
Novokhatskii and Lenev [23] (1966) Hino et al. [51] (1994)	gas mixing - H_2-H_2O gas mixing - CO-CO_2	1573 - 1773 K 1423 - 1723 K	-224.28 -214.04 ±1.75	linear extrapolation std. deviation recalc. (see text)
Rezukhina et al. [52] (1965)	emf - La_2O_3-ThO_2	1298 - 1433 K	-213.36 ±0.29	Fe-FeO ref
Tretjakow and Schmalzreid [25] (1965)	emf - CaO-ZrO_2	1000 - 1500 K	-205.71	air ref
Freuhan [53] (1969) Snethlage and Klemm [54] (1975)	emf - CaO-ZrO_2 emf - CaO-ZrO_2	1600°C 1273 - 1473 K	 -211.26	Cr-Cr_2O_3 ref Fe-FeO ref
Jacob and Alcock [55] (1975)	emf - Y_2O_3-ThO_2	1023 - 1809 K	-214.85 ±0.62	Fe-FeO buffer
Zabeivorota et al. [30] (1980) Nagata and Murohashi [56] (1990)	emf - Y_2O_3-ZrO_2 emf	1400 - 1780 K 1300 - 1500 K	-214.38 ±0.42 -217.88	Mo-MoO_2 and Fe/V_2O_3/FeV_2O_4 refs

[a]Gibbs energy change for reaction (15).

Table 9

Experimental Studies on the Stability of $CoCr_2O_4$

Reference	Technique	Temp. Range	$\Delta_f G°$(1373 K)[a] kJ mol^{-1}	Comments
Kunnmann et al. [49] (1963)	gas mixing - CO-CO_2	1073 - 1380 K	-181.42 ±1.05	
Aukrust and Muan [58] (1963)	gas mixing - CO-CO_2	1623 K	-166.11 ±2.51[b]	reversed
Lenev and Novokhatskii [59] (1966)	gas mixing - CO-CO_2	1273 - 1673 K	-183.51 ±1.26	
Koc and Timucin [61] (2005)	gas mixing - H_2-CO_2	1573 K		$\Delta_f G°$(1573 K) = -160.55 kJ mol^{-1}
Levitskii et al. [62] (1965)	emf - La_2O_3-ThO_2	1270 - 1490 K	-190.07 ±0.29	Fe-FeO ref
Tretjakow and Schmalzreid [25] (1965)	emf - CaO-ZrO_2	1000 - 1500 K	-184.85 ±0.84	air ref
Jacob and Fitzner [60] (1977)	emf - ??	1373 K	-186.79	unpublished data
Schaefer [63] (1986)	emf - CaO-ZrO_2	1173 - 1256 K		Cu-Cu_2O ref

[a]Gibbs energy change for reaction (26). [b]at 1623 K

Table 10

Thermodynamic coefficients for Cr_2O_3 and MCr_2O_4 compounds at 298.15 K

Species	$C_p°(298)$[a]	$S°(298)$[a]	$\Delta_f H°(298)$[b]	$\Delta_f G°(298)$[b]	Source
Cr(bcc)	23.47	23.54	0	0	c
O_2(g)	29.35	205.15	0	0	c
Fe(bcc)	25.08	27.28	0	0	c
Co(hcp)	24.81	30.04	0	0	c
Zn(s)	25.39	41.63	0	0	c
$FeCr_2O_4$(s)	133.86	152.2	-1438.52	-1339.40	This study
$ZnCr_2O_4$(s)	128.60	127.4	-1539.16	-1428.35	This study
$CoCr_2O_4$(s)	130.15	134.96	-1431.84	-1326.75	This study
Cr_2O_3(s)	127.08	82.3	-1131.21	-1049.96	This study

[a]units J-mol^{-1}-K^{-1}, [b]units kJ-mol^{-1}, [c] Dinsdale [13]

Table 11

Heat Capacity Anomalies in Transition Metal Chromites and Ferrites

M	MCr_2O_4 Neel Temp., K	Residual LT Anomaly, K	MFe_2O_4 Curie Temp., K	Residual LT Anomaly, K
Fe[a]	36.5	68.7	858	--
Co	24	95.1	793	~90
Ni[a]	29	75	858	~90
Zn	12.3	--	9.5[b]	75

[a]Third thermal anomaly is present due to structural transition in $FeCr_2O_4$ (at 124.1 K), Fe_3O_4 (at 123.8 K) and $NiCr_2O_4$ (at 310 K).
[b]Neel temperature.

List of Figures

Fig. 12. Deviation plot of Gibbs energies of Cr_2O_3 formation derived from high temperature emf and gas mixing data over the temperature ranges of the experiments relative to values provided by the present thermodynamic extrapolation. Also shown are deviations relative to predictions based on the previous recommendations of Chase [40]: $\Delta_f G°(298) = -1053.11$ kJ mol^{-1} and $S°(298) = 81.15$ J mol^{-1} K^{-1}.

Fig. 13. Gibbs energies of $FeCr_2O_4$ formation from Fe, O_2 and Cr_2O_3 derived from the published experimental data over the ranges of the experiments. Also shown is our thermodynamic extrapolation for reaction (15).

Fig. 14. Deviation plot of Gibbs energies of $FeCr_2O_4$ formation derived from high temperature emf and gas mixing data over the temperature ranges of the experiments relative to values provided by the present thermodynamic extrapolation. Deviations relative to Barin-compiled properties [1] for reaction (15): $\Delta_f G°(298) = -297.82$ kJ mol^{-1} and $\Delta_f S°(298) = -69.09$ J mol^{-1} K^{-1} are also shown.

Fig. 15. Gibbs energies of $ZnCr_2O_4$ formation from ZnO and Cr_2O_3, reaction (22). The thermodynamic extrapolation deviates from high temperature measurements by <0.03 kJ mol^{-1}.

Fig. 16. Gibbs energies of $CoCr_2O_4$ formation from Co, O_2 and Cr_2O_3 derived from the published experimental data over the temperature ranges of the experiments. The predicted location for reaction (26) is also shown based on our thermodynamic extrapolation.

Fig. 17. Deviation plot of Gibbs energies of $CoCr_2O_4$ formation derived from high temperature emf and gas mixing data over the temperature ranges of the experiments relative to values provided by the present thermodynamic extrapolation. Deviations relative to Barin-compiled [1] properties for reaction (26): $\Delta_f G°(298) = -271.71$ kJ mol^{-1} and $\Delta_f S°(298) = -87.46$ J mol^{-1} K^{-1} are also shown.

Fig. 18. Comparison of high-temperature heat capacities of transition metal chromites and ferrites. The heat capacities are made dimensionless by dividing by the limiting lattice vibrational contribution to C_V, which is 21R for MCr_2O_4 and MFe_2O_4, and 15R for Cr_2O_3. Data for $NiCr_2O_4$ taken from Chizhikov et al. [66].

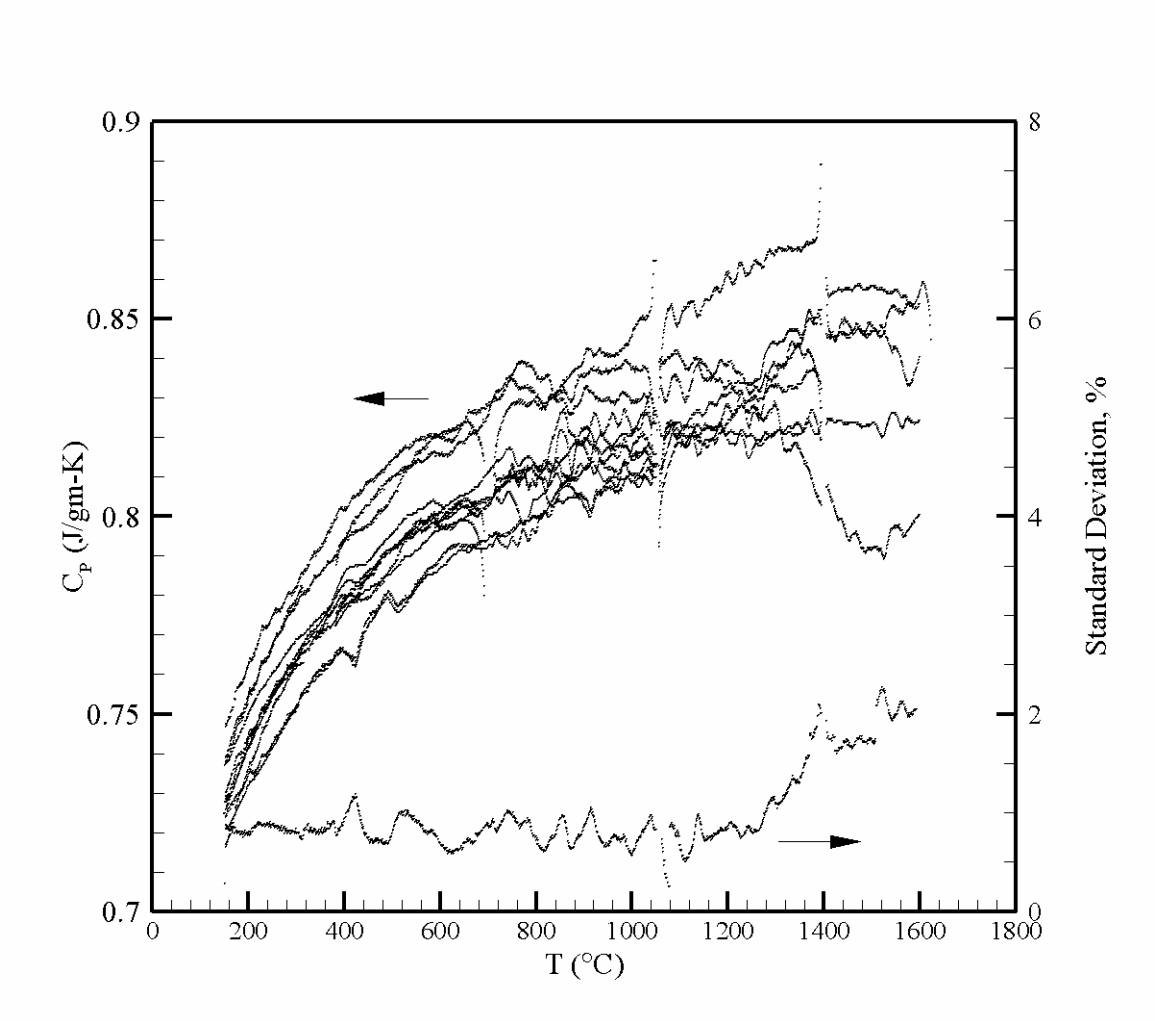

Fig. 1. Raw, high-temperature C_P data for Cr_2O_3 showing root-mean-square deviation as a function of temperature.

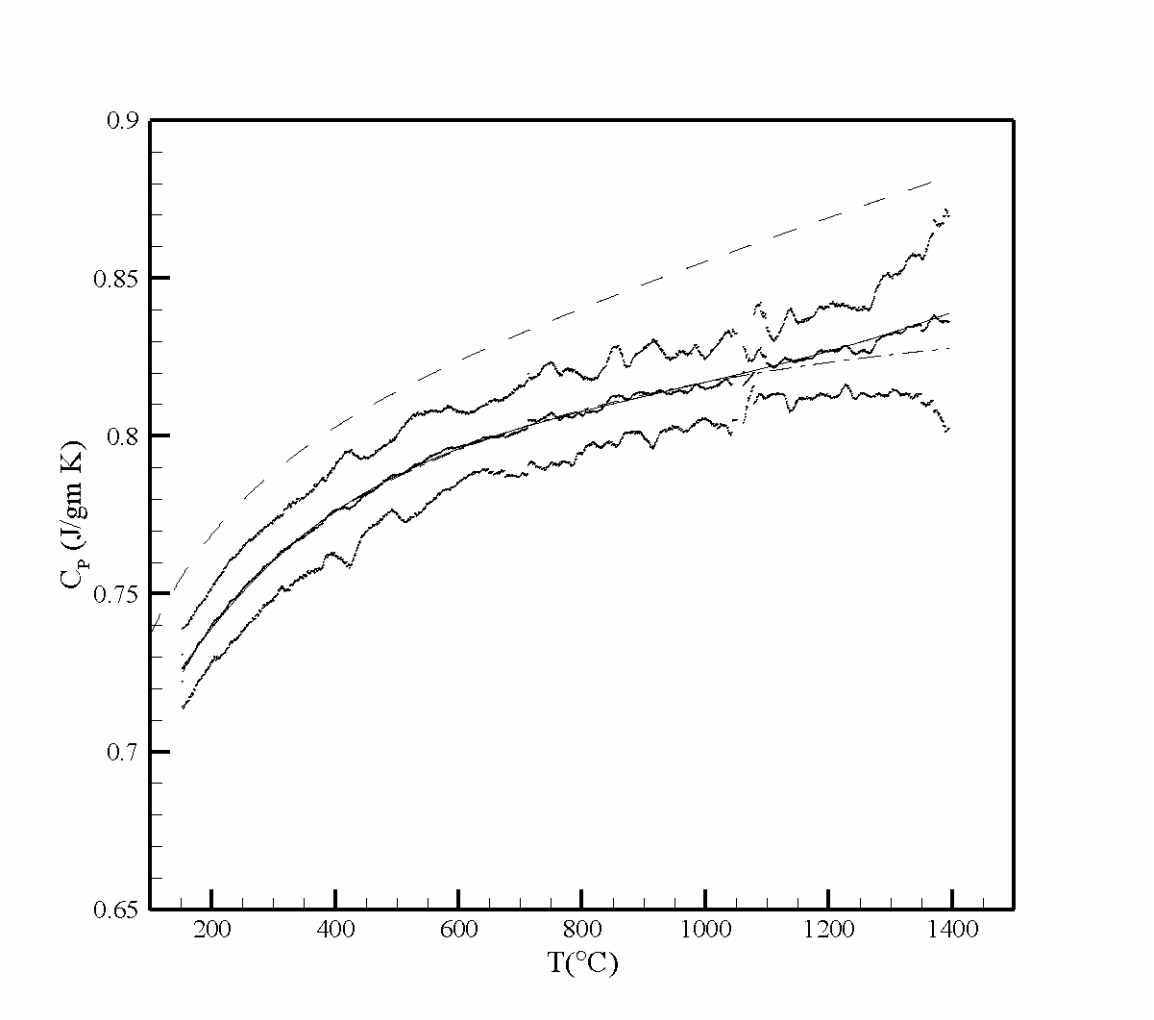

Fig. 2. Summary of the high-temperature C_P data for Cr_2O_3, showing the average values and " two sigma limits. A smoothed curve (dot-dash) is also drawn based on a fit to the data below 1050°C, with an additional point added at 2000°C to prevent high-temperature deviations. Previous measurements of Moore and Kelley [39] shown as a dashed line.

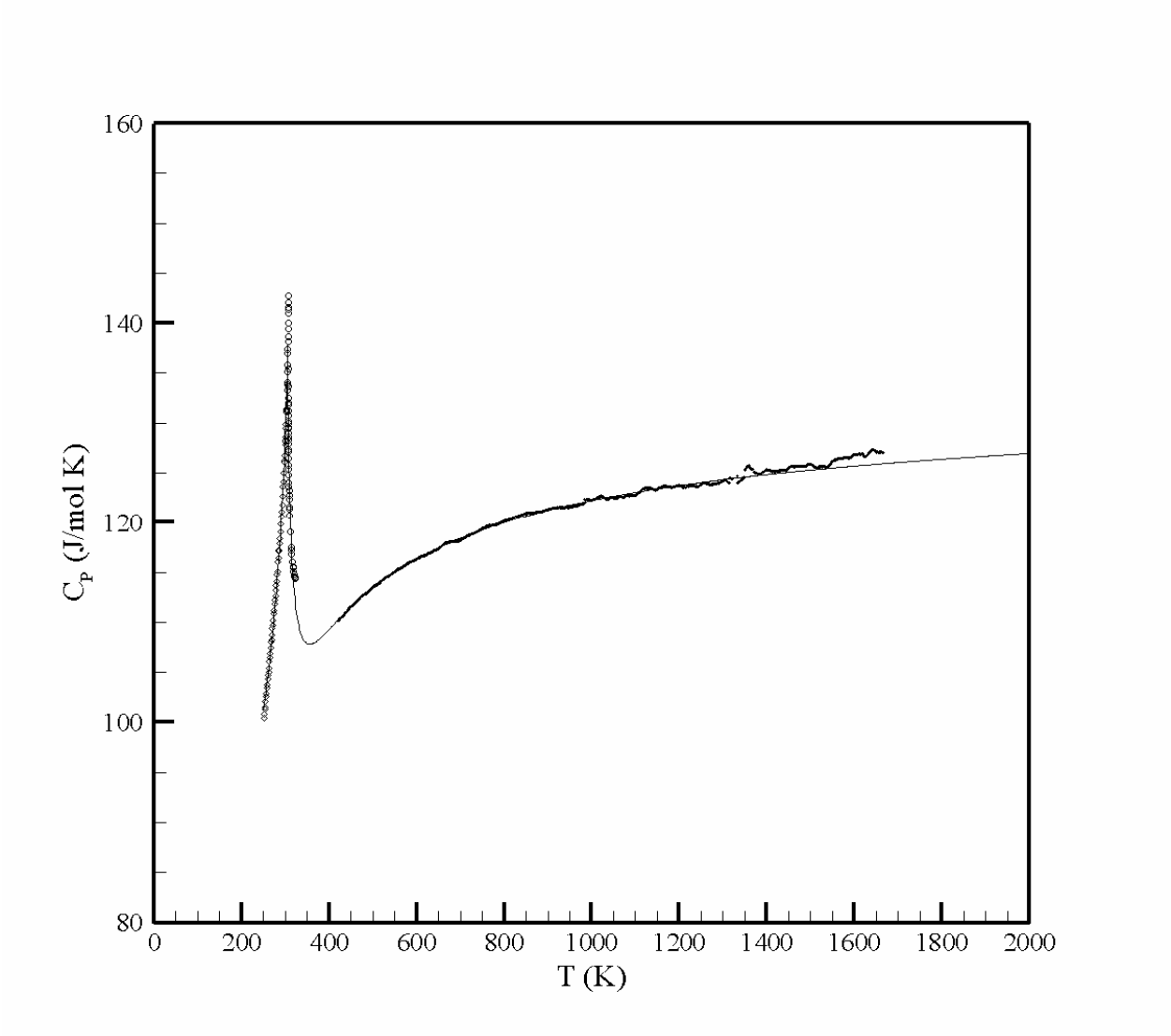

Fig. 3. Summary of ambient and high temperature C_P data for Cr_2O_3. Data below 400 K are taken from Klemme et al. [3] and Bruce and Cannell [11], as discussed in text. Parameters for fitted curve are given in Table 2.

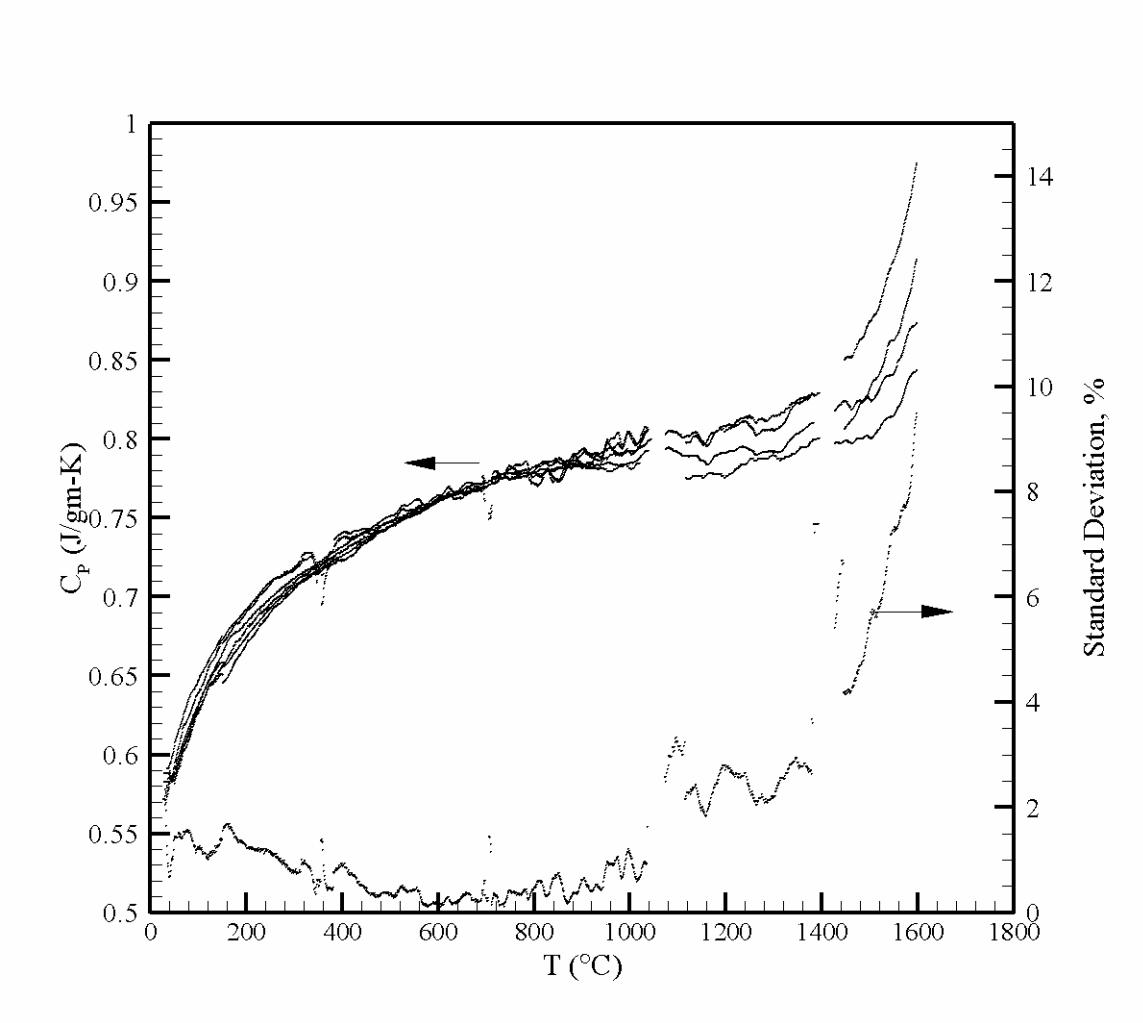

Fig. 4. Raw, high-temperature C_P data for $FeCr_2O_4$ showing root-mean-square deviation as a function of temperature.

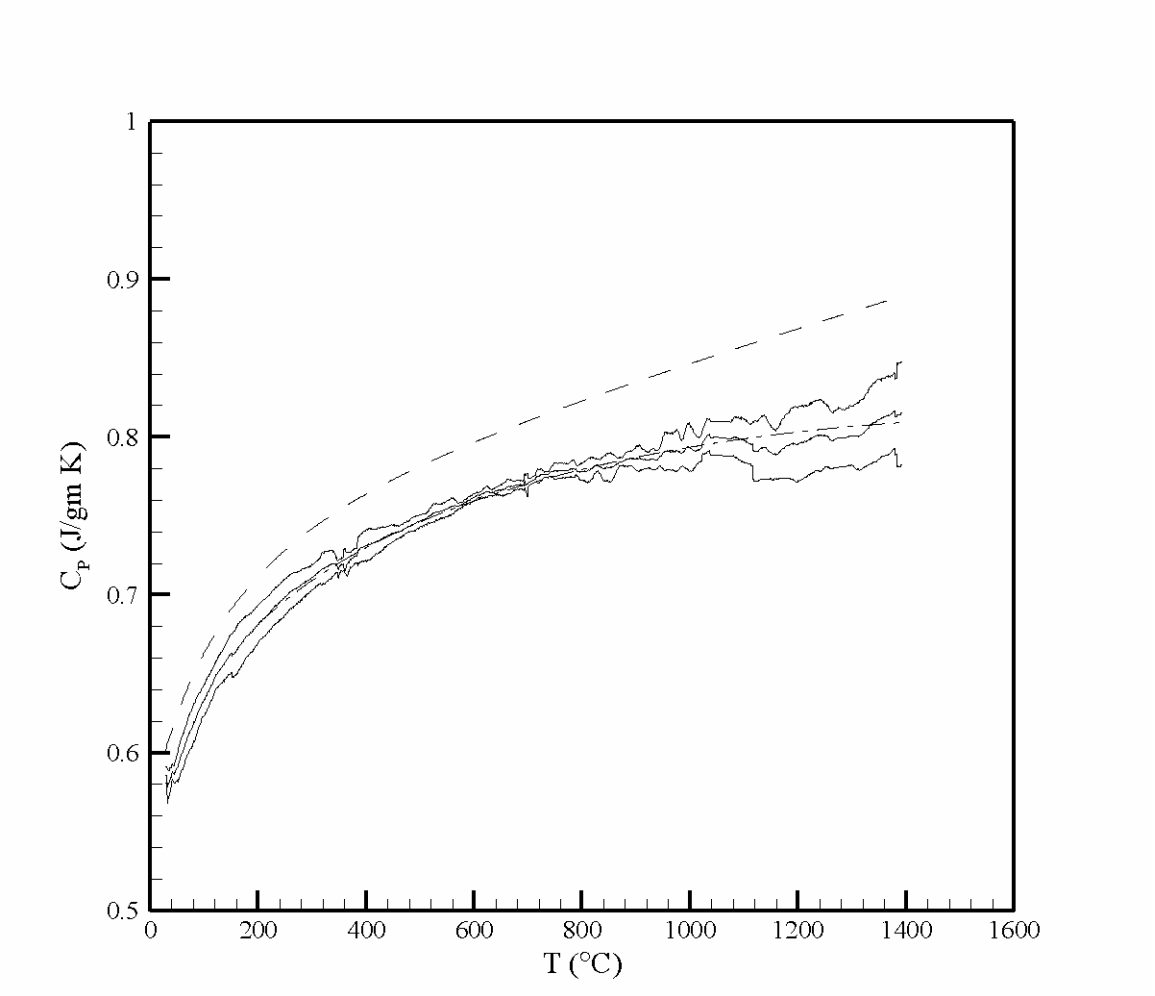

Fig. 5. Summary of high-temperature C_P data for $FeCr_2O_4$, showing the average values " two sigma limits. A smoothed curve is included based on a fit to the data below 1050°C, with a constraint imposed at 1727°C to ensure smooth extrapolation to higher temperatures. Previous measurements of Naylor [15] shown as a dashed line.

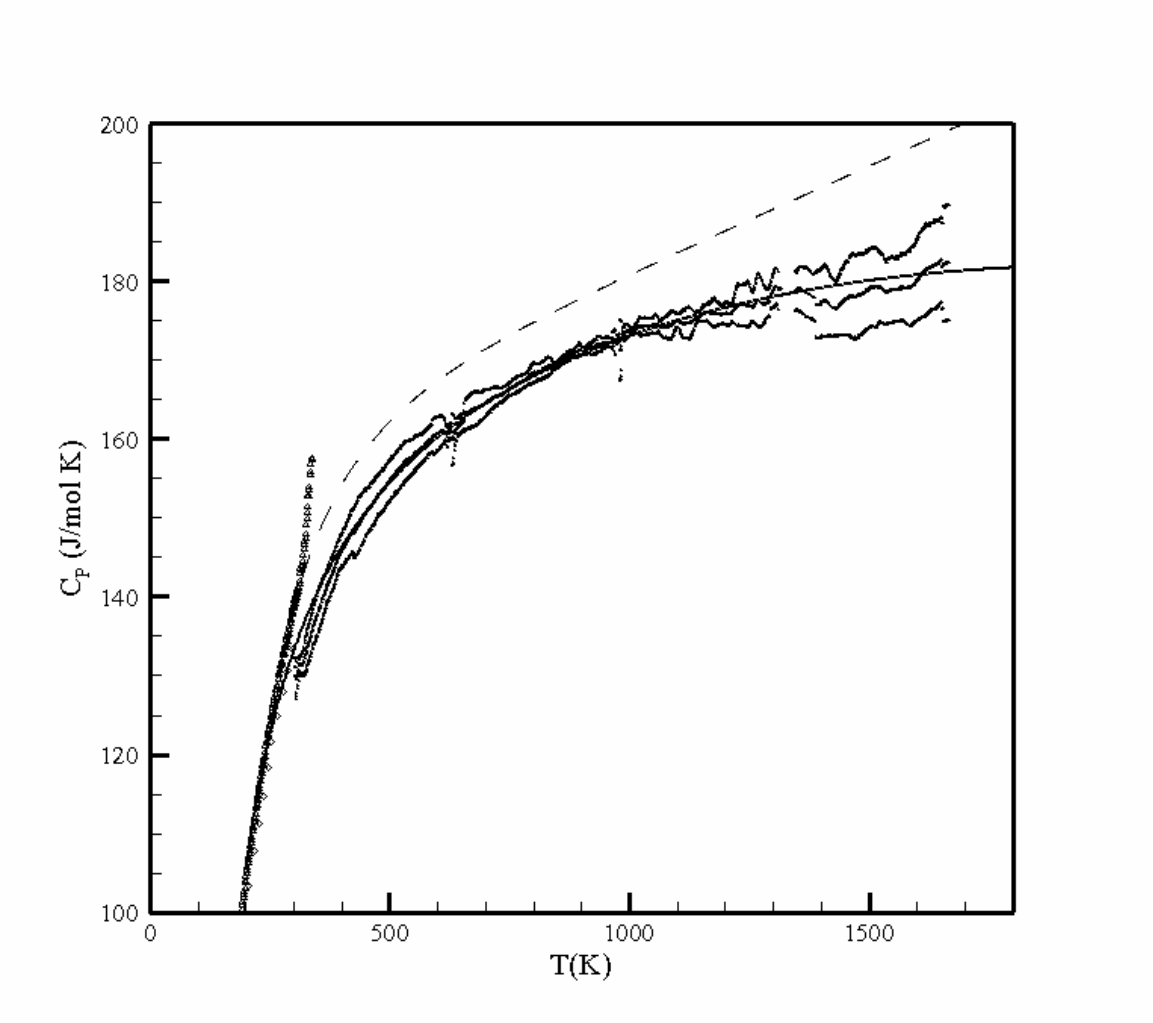

Fig. 6. Comparison of low- and high-temperature heat capacities of $FeCr_2O_4$: low-temperature data from Klemme et al. [3] and Shomate [17]; high-temperature results from present DSC data ± two sigma limits. Naylor [15] results shown as dashed line.

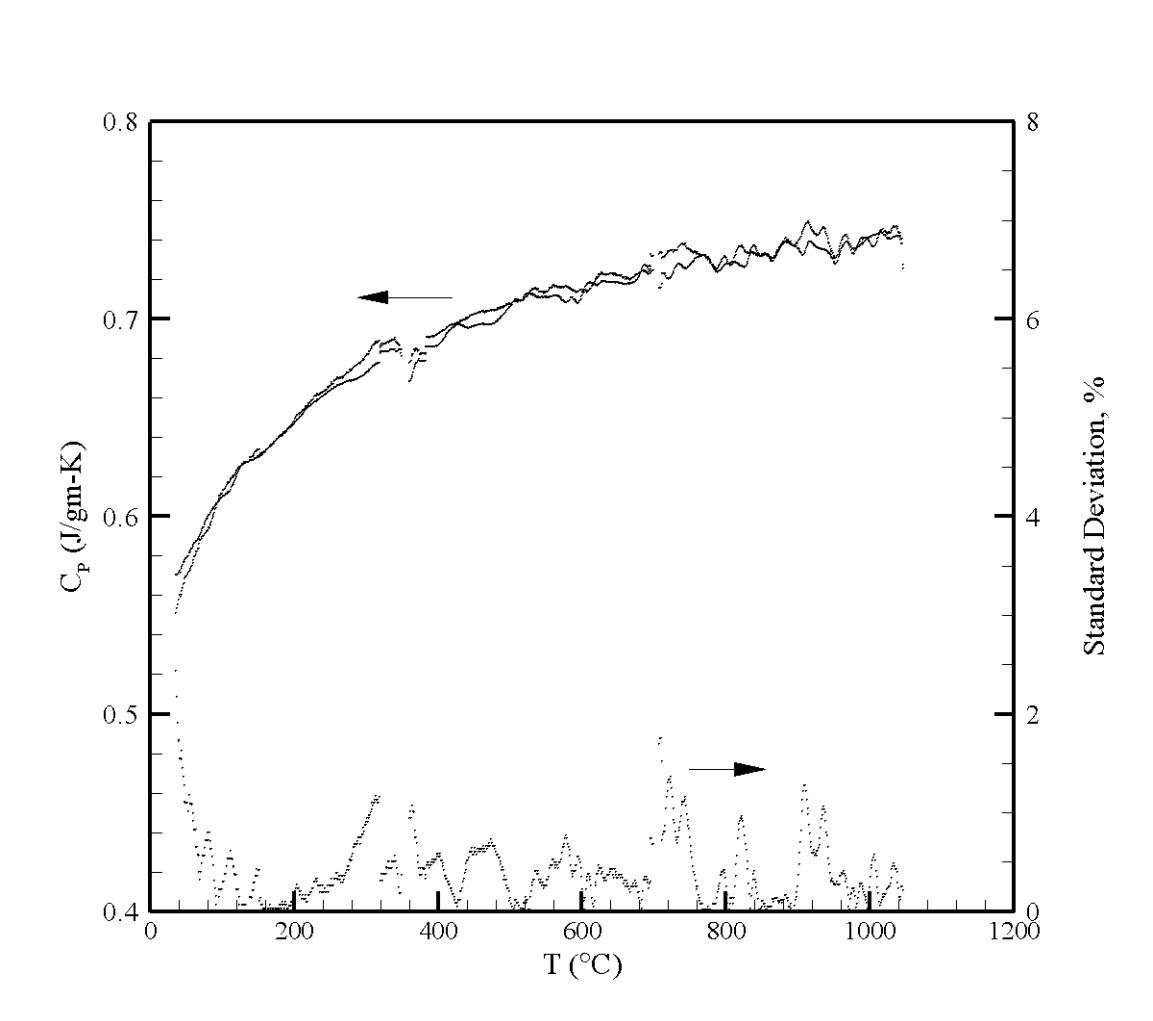

Fig. 7. Raw, high-temperature C_P data for $ZnCr_2O_4$ showing root-mean-square deviation as a function of temperature.

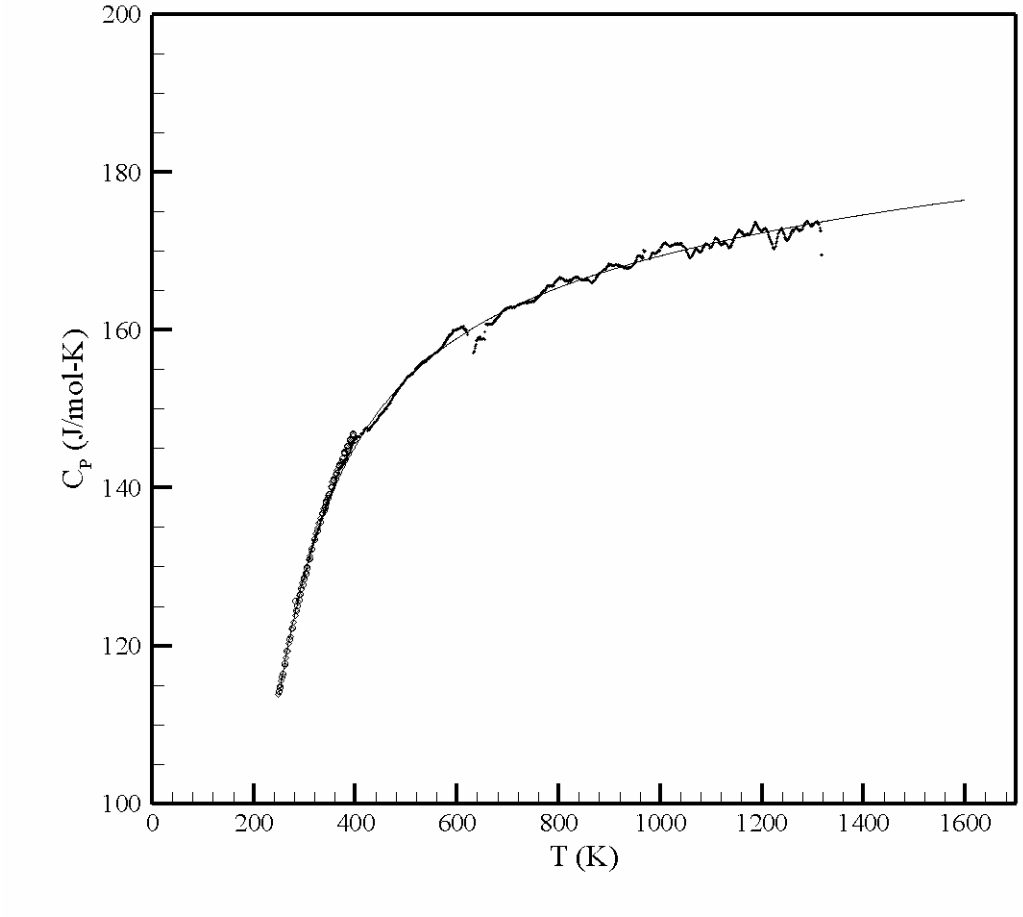

Fig. 8. Fitted $C_P(T)$ curve for $ZnCr_2O_4$ overlain on the truncated low-temperature [6] and DSC average high-temperature data. Maier-Kelley parameters for fitted curve are given in Table 2.

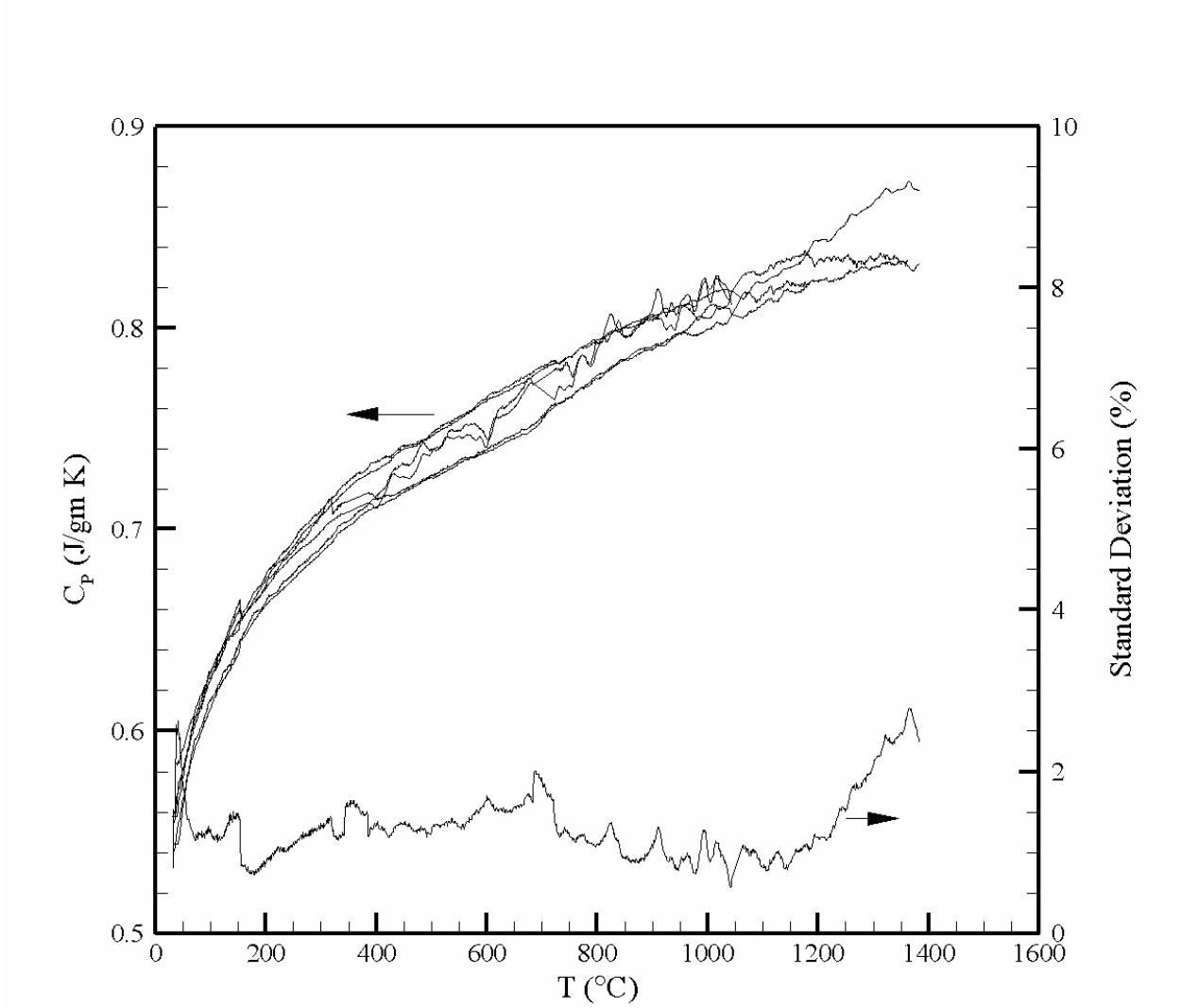

Fig. 9. Raw, high-temperature C_P data for $CoCr_2O_4$ showing root-mean-square deviation as a function of temperature.

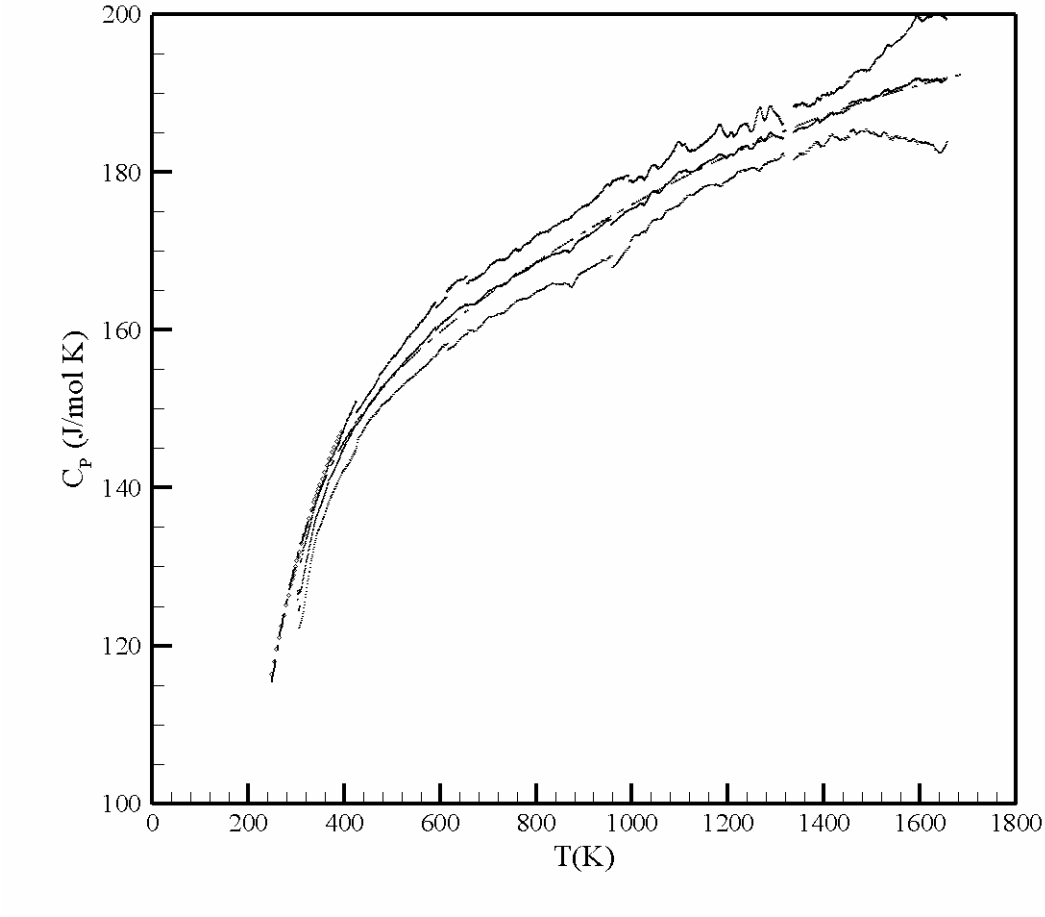

Fig. 10. Comparison of low- and high-temperature C_P data for $CoCr_2O_4$: low-temperature, adiabatic calorimetric results from Ref. [7]; high-temperature results are present DSC measurements ± two sigma limits. Fitted $C_P(T)$ curve includes data between 250 and 1657 K, with a constraint imposed to permit smooth extrapolation to 2000 K.

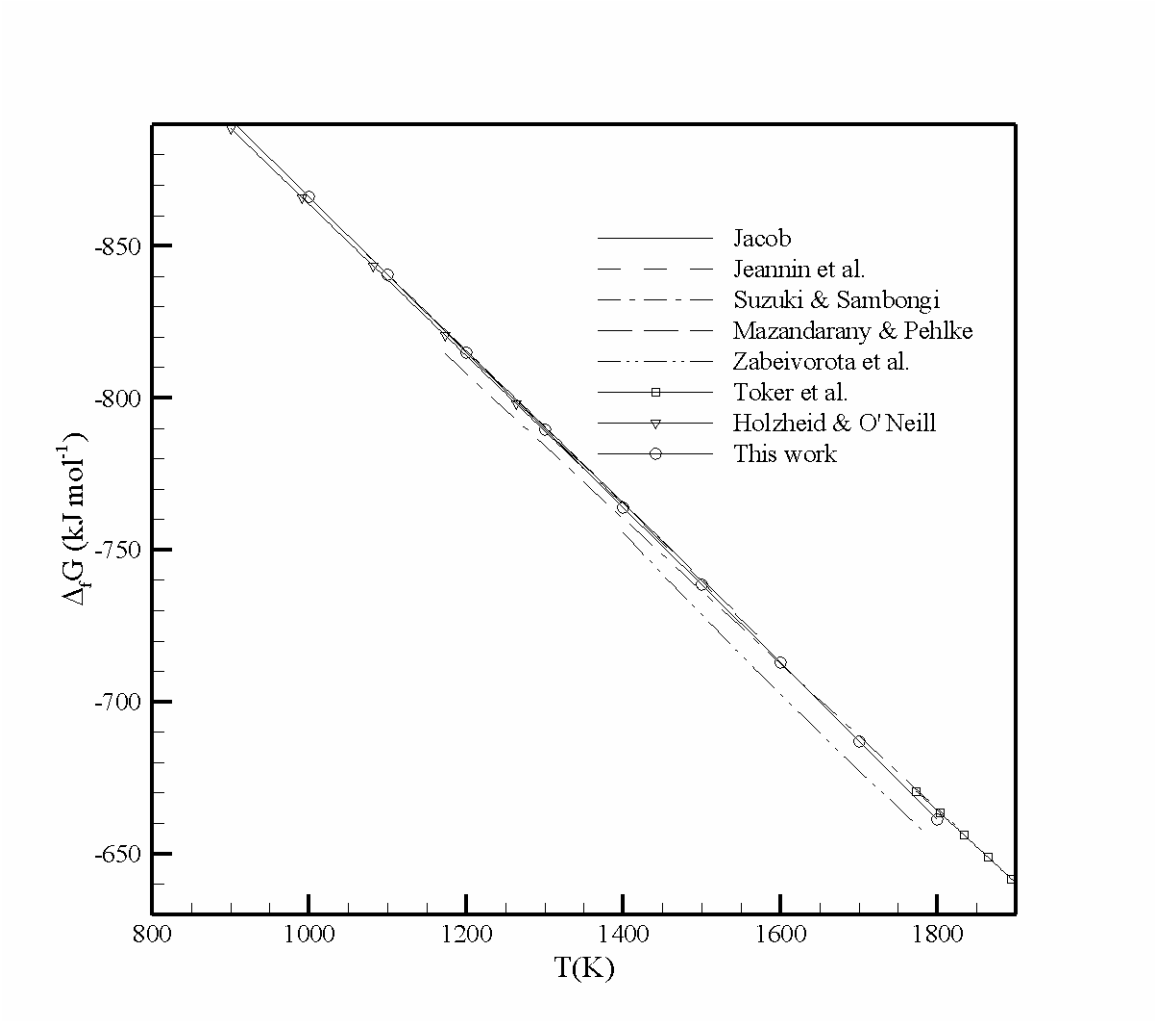

Fig. 11. Gibbs energies of Cr_2O_3 formation from Cr and O_2 derived from the published experimental data over the temperature ranges of the experiments. Also shown is the predicted location for reaction (14) based on our thermodynamic extrapolation.

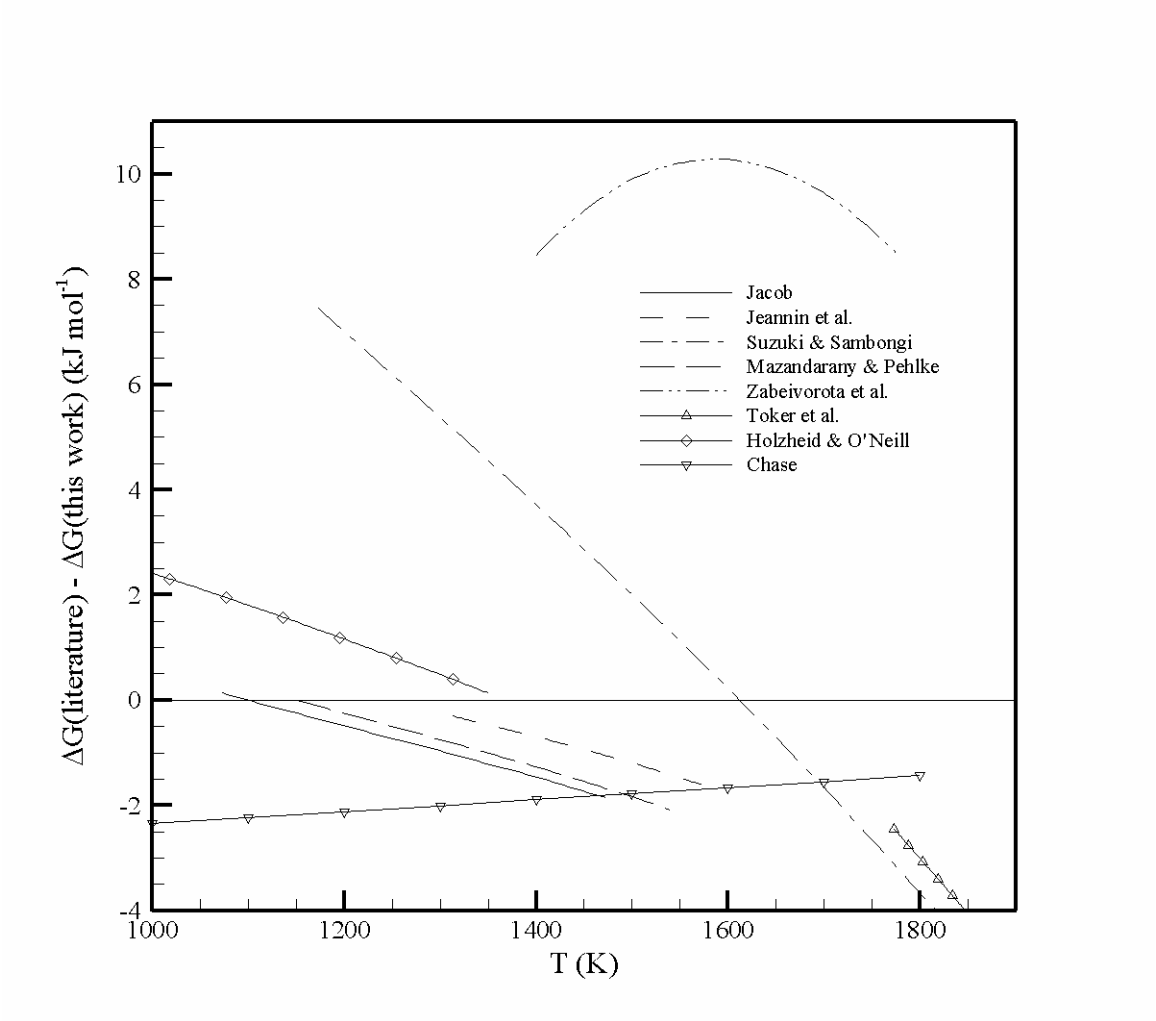

Fig. 12. Deviation plot of Gibbs energies of Cr_2O_3 formation derived from high temperature emf and gas mixing data over the temperature ranges of the experiments relative to values provided by the present thermodynamic extrapolation. Also shown are deviations relative to predictions based on the previous recommendations of Chase [40]: $\Delta_f G°(298) = -1053.11$ kJ mol^{-1} and $S°(298) = 81.15$ J mol^{-1} K^{-1}.

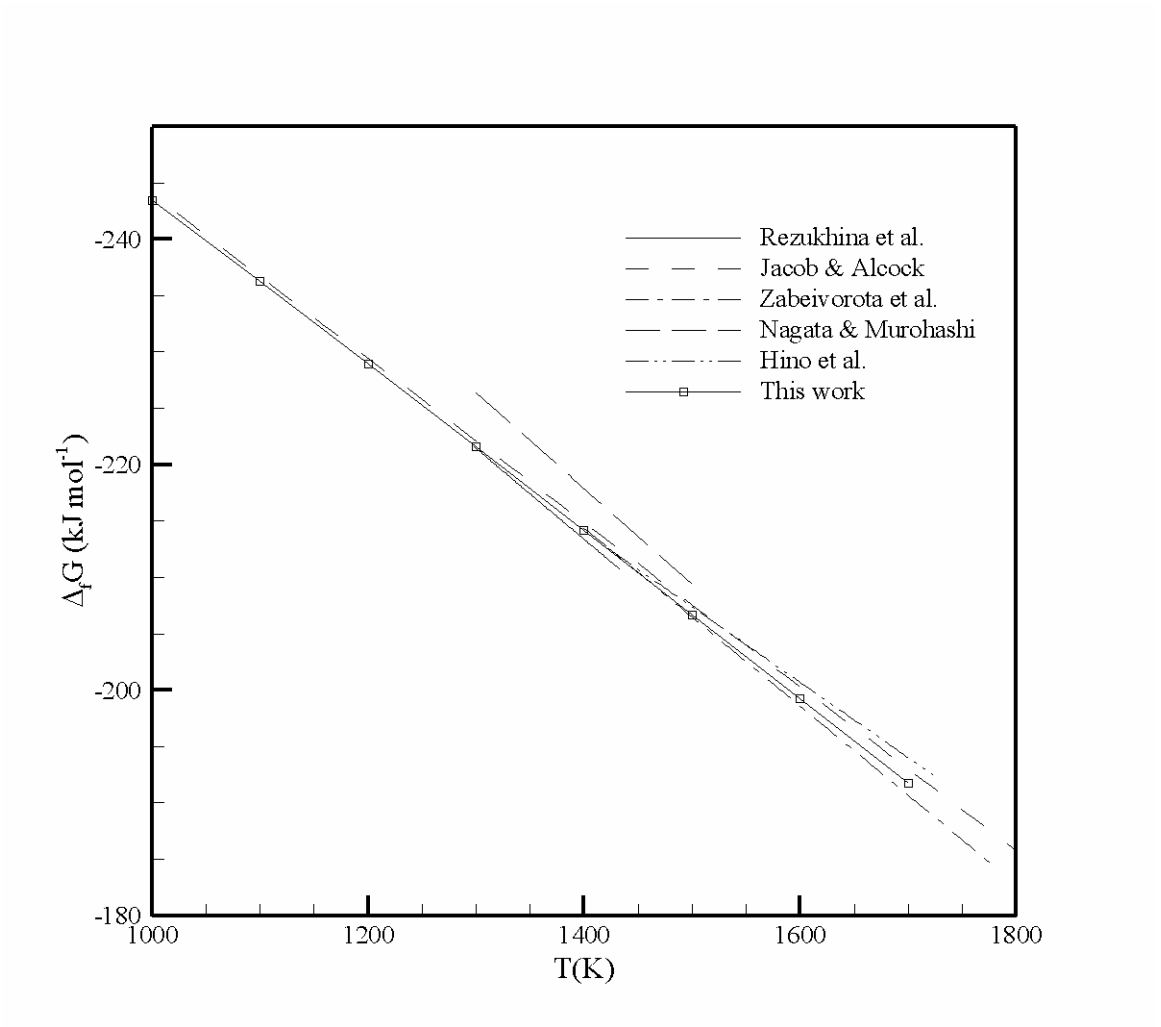

Fig. 13. Gibbs energies of $FeCr_2O_4$ formation from Fe, O_2 and Cr_2O_3 derived from the published experimental data over the ranges of the experiments. Also shown is our thermodynamic extrapolation for reaction (15).

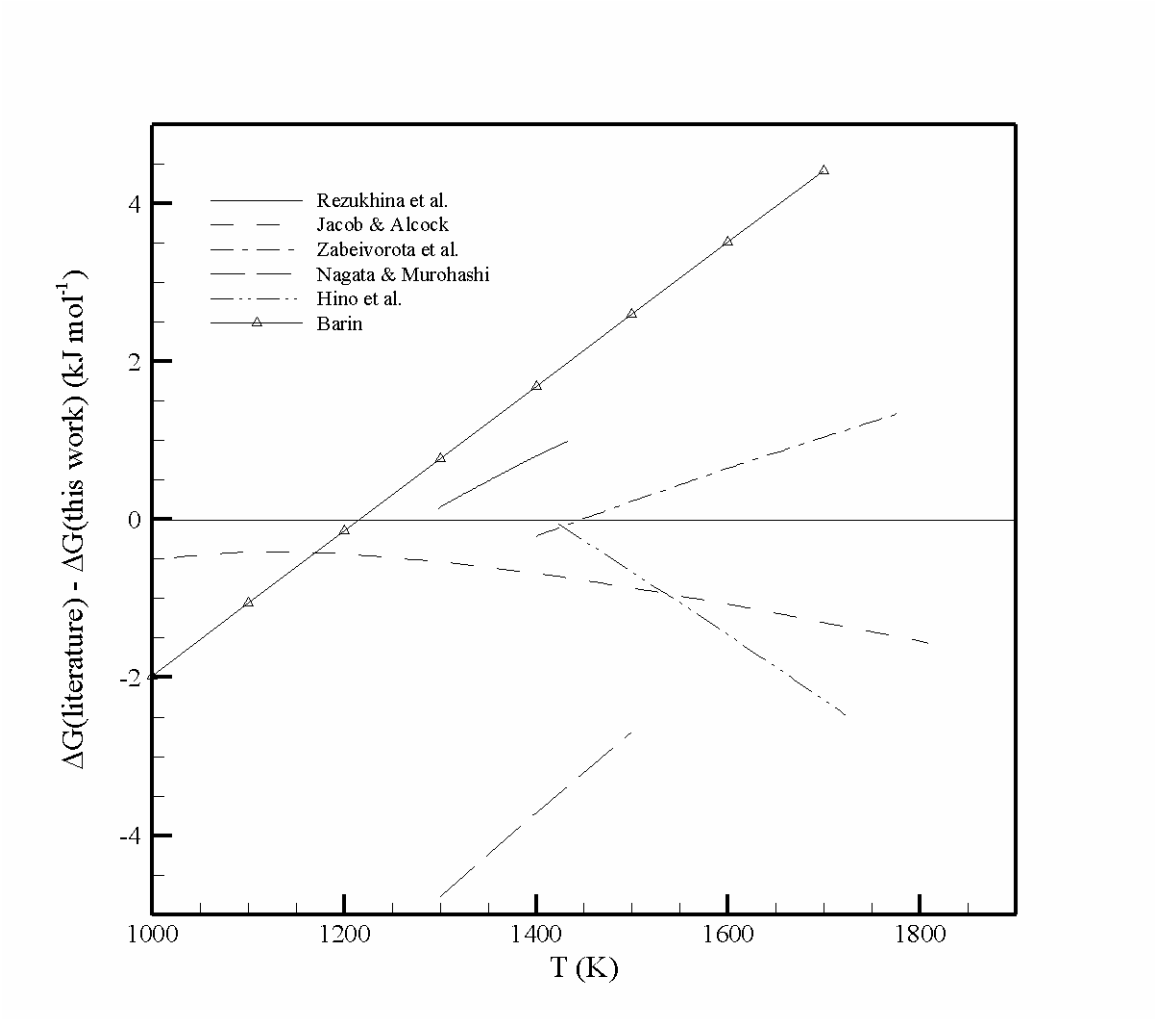

Fig. 14. Deviation plot of Gibbs energies of $FeCr_2O_4$ formation derived from high temperature emf and gas mixing data over the temperature ranges of the experiments relative to values provided by the present thermodynamic extrapolation. Deviations relative to Barin-compiled [1] properties for reaction (15): $\Delta_f G°(298) = -297.82$ kJ mol^{-1} and $\Delta_f S°(298) = -69.09$ J mol^{-1} K^{-1} are also shown.

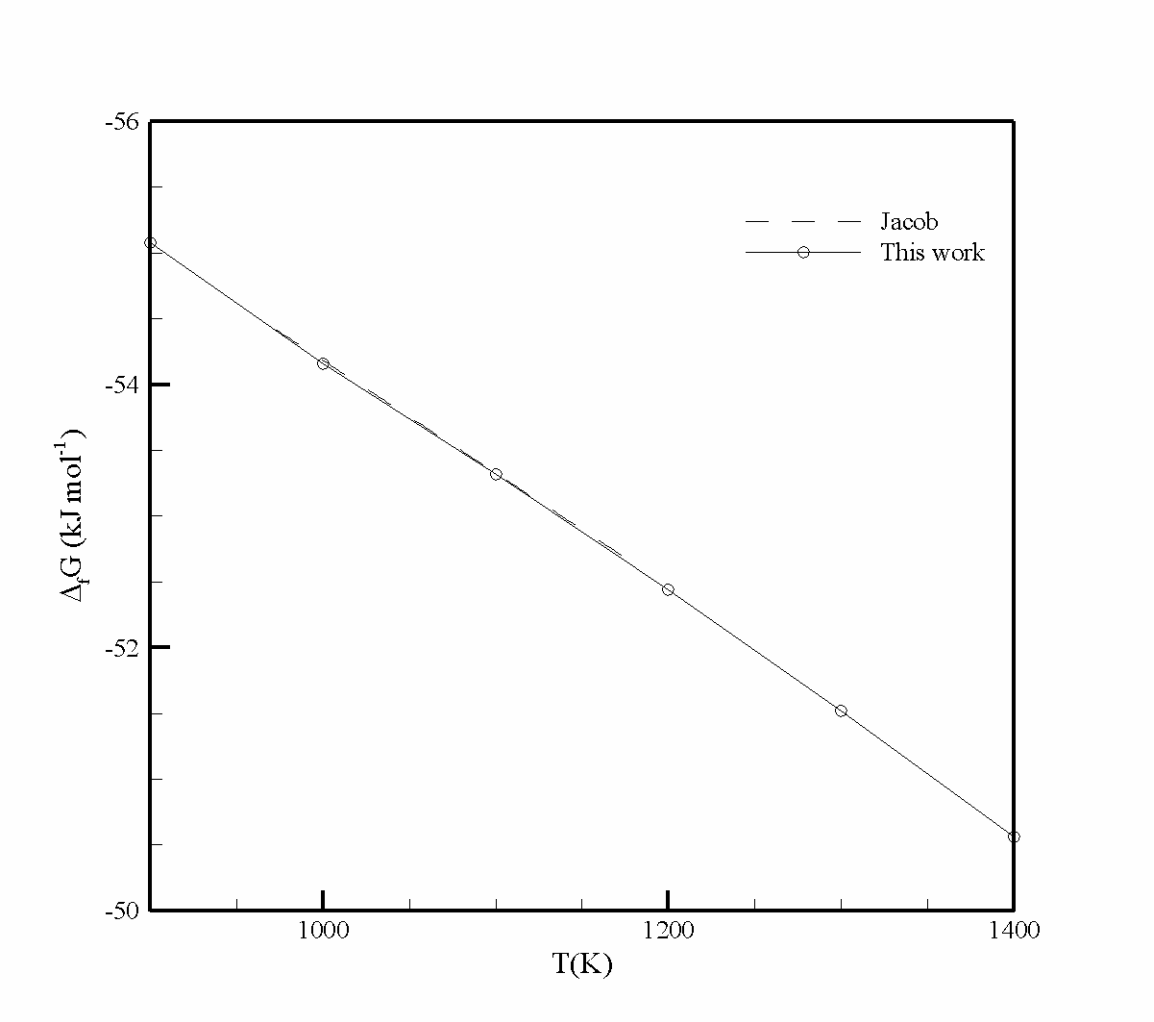

Fig. 15. Gibbs energies of $ZnCr_2O_4$ formation from ZnO and Cr_2O_3, reaction (22). The thermodynamic extrapolation deviates from high temperature measurements by <0.03 kJ mol^{-1}.

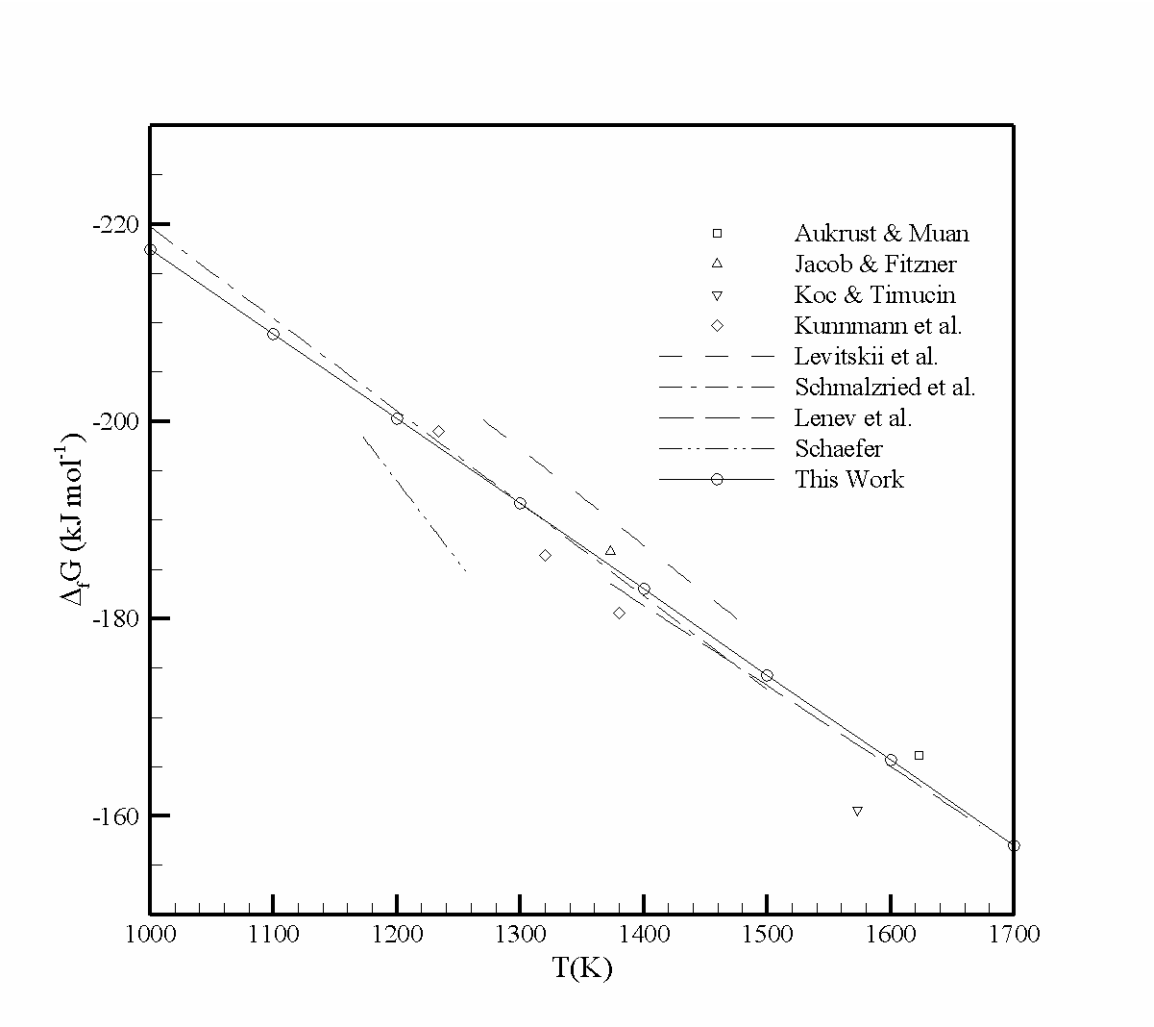

Fig. 16. Gibbs energies of $CoCr_2O_4$ formation from Co, O_2 and Cr_2O_3 derived from the published experimental data over the temperature ranges of the experiments. The predicted location for reaction (26) is also shown based on our thermodynamic extrapolation.

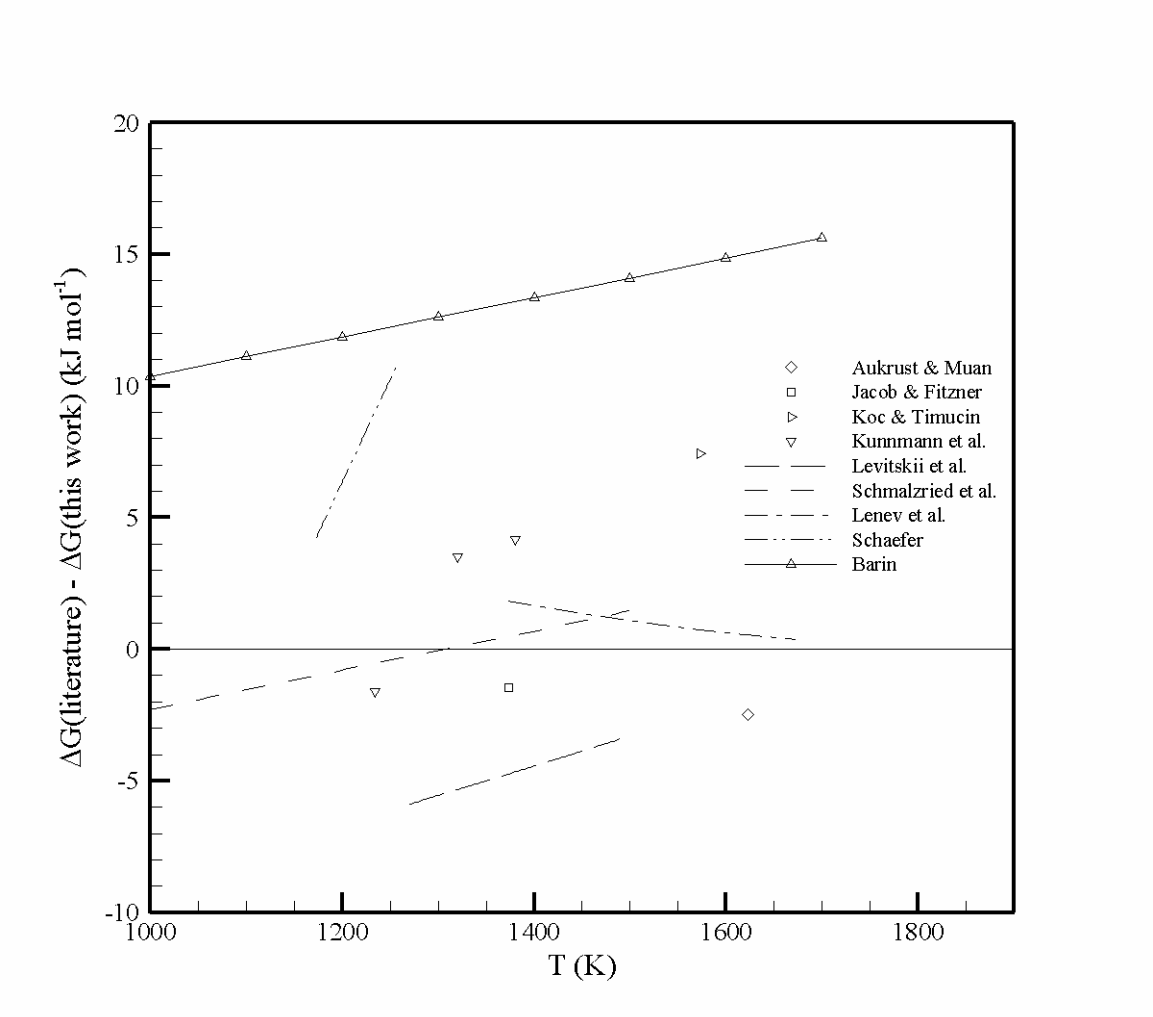

Fig. 17. Deviation plot of Gibbs energies of $CoCr_2O_4$ formation derived from high temperature emf and gas mixing data over the temperature ranges of the experiments relative to values provided by the present thermodynamic extrapolation. Deviations relative to Barin-compiled [1] properties for reaction (26): $\Delta_f G°(298) = -271.71$ kJ mol^{-1} and $\Delta_f S°(298) = -87.46$ J mol^{-1} K^{-1} are also shown.

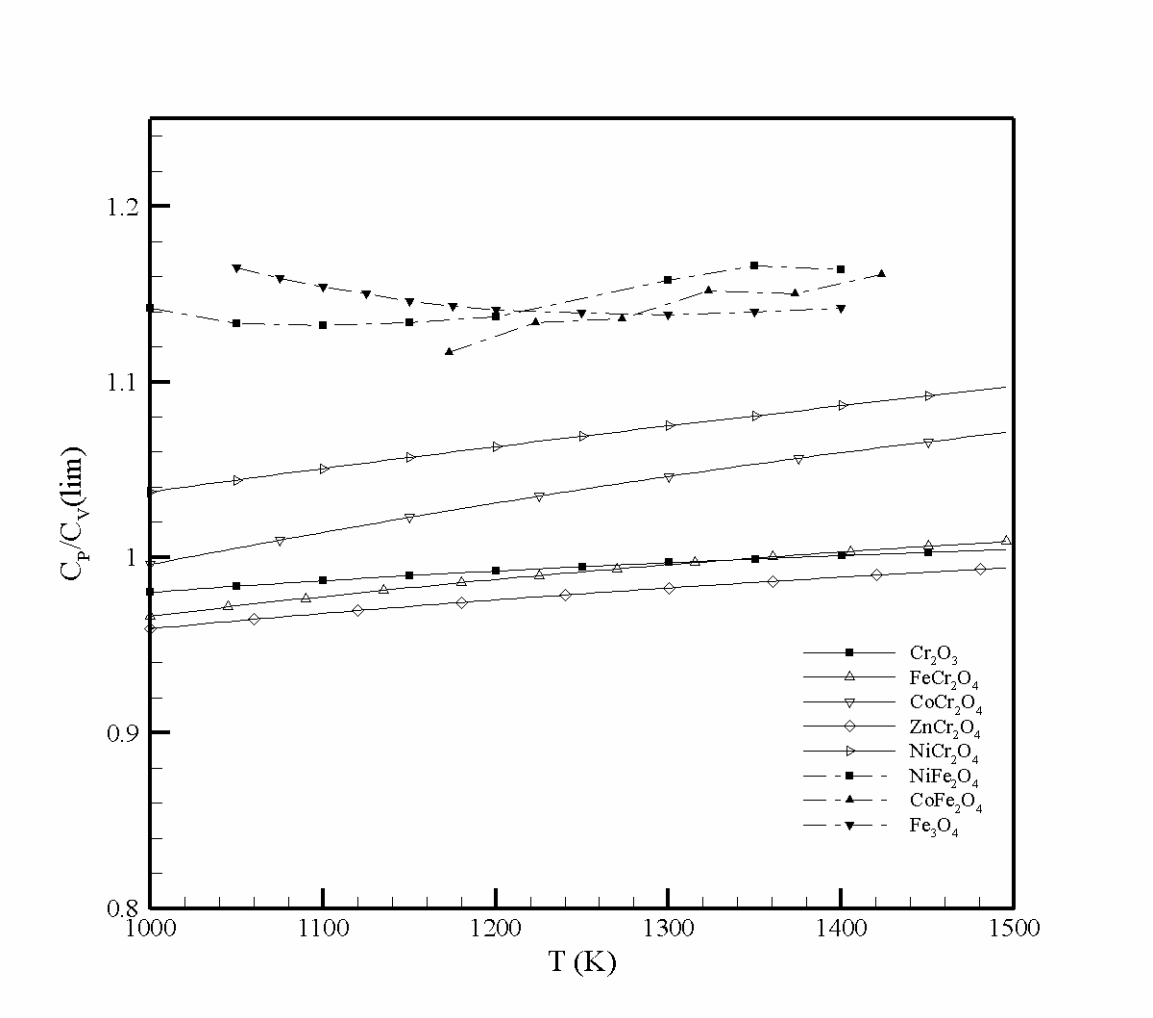

Fig. 18. Comparison of high-temperature heat capacities of transition metal chromites and ferrites. The heat capacities are made dimensionless by dividing by the limiting lattice vibrational contribution to C_V, which is 21R for MCr_2O_4 and MFe_2O_4, and 15R for Cr_2O_3. Data for $NiCr_2O_4$ taken from Chizhikov et al. [66].